UNIVERSITÀ DEGLI STUDI DI MILANO

FACOLTÀ DI SCIENZE E TECNOLOGIE

PhD course in Molecular and Cellular Biology

XXXI Cycle

HCN domain: a key regulator of HCN channel gating

Alessandro Porro

Scientific tutor: Prof. Anna Moroni

Academic year: 2018/2019

Index

Abstract (italiano)

I canali ionici sono proteine trans-membrana che si assemblano per formare pori selettivi che mediano il passaggio di specie ioniche dall'interno all'esterno delle cellule e viceversa. I canali HCN sono una classe di canali voltaggio dipendenti (HCN1 – HCN4) che mediano la corrente I_f nel tessuto cardiaco e la corrente I_h nel sistema nervoso centrale, dove regolano processi fisiologici importanti tra cui il ritmo cardiaco, l'integrazione dendritica e la percezione del dolore [1], [2]. Dal punto di vista strutturale i canali HCN sono formati da una porzione transmembrana, che include il sensore del voltaggio e il dominio del poro, e una porzione C-terminale citosolica che contiene il sito di legame ai nucleotidi ciclici (CNBD, cyclic nucleotide binding domain) fisicamente connesso al poro tramite un dominio chiamato C-linker [3]. I canali HCN possiedono caratteristiche uniche nell'ambito dei canali ionici: sono attivati dall'iperpolarizzazione del potenziale di membrana (che permette l'apertura del poro consentendo il flusso ionico) e sono, allo stesso tempo, regolati dal legame ai nucleotidi ciclici al loro dominio CNBD che facilita l'aperura del poro spostando la relazione "probabilità di apertura/potenziale di membrana" verso potenziali più depolarizzati [2]. Nonostante i numerosi studi condotti negli ultimi 27 anni, il meccanismo molecolare che permette questa duplice regolazione non è ancora completamente conosciuto. La conoscenza di questi meccanismi è importante, in quanto la mancata regolazione del meccanismo di gating di questi canali è alla base dell'insorgenza di gravi patologie sia cardiache che neuronali [4], [5].
Recentemente, la struttura tridimensionale dell'intero tetramero dell'isoforma HCN1 è stata risolta per Cryo-EM [3], gettando le basi per un nuovo studio volto alla ricerca del meccanismo che permette la duplice regolazione. Combinando mutagenesi sito-diretta (sulla base di quanto osservato nella struttura pubblicata) ed esperimenti di elettrofisiologia, abbiamo individuato nel dominio N-terminale "HCN domain" l'elemento chiave che permette di mediare l'attivazione da voltaggio e la modulazione da nucleotidi ciclici nei canali HCN1 e HCN2, identificando le interazioni fondamentali che sono coinvolte. Sulla base di questa scoperta, abbiamo inoltre preparato un peptide sintetico, derivato dall' HCN domain, che, quando somministrato al canale, è in grado di modularne il gating mimando l'effetto del cAMP. Pertanto i risultati ottenuti non rappresentano solo un importante contributo per la comprensione del meccanismo di gating di questi canali, ma gettano anche le basi per lo sviluppo di farmaci basati su molecole o peptidi sintetici HCN specifici che regolano le correnti HCN sia nel cuore sia nel sistema nervoso.

Abstract

Hyperpolarization-activated and cyclic nucleotide–gated (HCN1-4) channels control key physiological functions such as cardiac pacemaking and repetitive neuronal firing [2]. Their molecular architecture comprises a voltage sensor and a pore domain that are membrane-embedded and a cytosolic soluble part that includes the cyclic nucleotide binding domain (CNBD) connected to the pore via a C-linker [3]. These channels are primarily activated by hyperpolarizing membrane voltage that opens the pore allowing the flux of a slow time-dependent depolarizing inward current known as I_f and I_h in the heart and in the brain, respectively [2]. HCN channels can be further regulated by the direct binding of cyclic nucleotides to the CNBD that enhances channel opening by shifting the relationship between opening and membrane hyperpolarization to more positive potentials [2]. Current knowledge of their mechanism of gating includes a downward movement/rotation of the voltage sensor that allosterically increases the affinity for cAMP in the CNBD, suggesting a direct interaction between the voltage sensor domain and the CNBD [6], [7]. The recently published single particle cryo-EM structure of HCN1 channel [3], constitutes the basis for this project that aims at understanding the cAMP-induced conformational changes leading to channel modulation. These are important questions to address because aberrant gating can lead to heart failures or epileptic seizures [8], [9].

Interestingly, the high resolution HCN1 structure shows that the N-terminus forms a 3 alfa-helical domain, called HCN domain. In the tetrameric assembly of the full length channel, the HCN domain of one subunit is inserted between the voltage sensor and the C-linker of the adjacent subunit [3]. This suggests that the HCN domain could be the element coupling the cyclic nucleotide regulation whit the voltage sensitivity. By a combination of rational mutagenesis and functional analysis of the ion currents by patch-clamp, we found that the newly discovered HCN domain plays a crucial role in the modulation of the voltage dependence of the channel as well as in the cAMP response. Moreover, we show that by interacting with the CNBD in HCN2 but not in HCN1, the HCN domain regulates the affinity of the channel for the ligand.

On the basis of these results we have prepared a synthetic HCN domain peptide that, when added to the channel, mimics the effect of cAMP.

These promising results contribute not only to a better understating of the gating mechanism of the channel but also lay the basis for the design of drug molecules able to modulate HCN-mediated currents both in nervous system and heart.

1 INTRODUCTION

1.1 HCN channels

Hyperpolarization-activated, cyclic nucleotide–gated (HCN) channels are important members of the voltage-gated pore loop channels family [2]. As previously postulated and recently confirmed by the high resolution cryo-EM structure of human HCN1 channel, the core unit is composed by the assembly of four subunits embedded in the plasma membrane to create an ion conducting pore [3]. In mammals four different isoforms (HCN1-HCN4) were found to be differently expressed in the central and peripheral nervous system as well as in the heart where they are able to form both homo- and heterotetramers [10]. HCN1 is expressed in the neo- cortex, hippocampus, cerebellar cortex as well as HCN1 expression was reported in the spinal cord. HCN2 is distributed ubiquitously in most brain regions with the highest expression in the thalamus [11]. By contrast, HCN3 is sparsely distributed at very low levels in the central nervous system. Relevant expression levels were only detected in the olfactory bulb and in some hypothalamic nuclei [12]. HCN4 expression is restricted in some parts of the brain such as in various thalamic nuclei and in the mitral cell layer of the olfactory bulb while in other brain regions the expression of HCN4 is much lower [12], [13]. In the peripheral nervous system all four HCN subtypes have been reported in the dorsal root ganglion, with HCN1 being the most abundant one [12]. All four HCN channel subtypes are present in the mammalian heart where the dominant subtype is HCN4, accounting for approximately 80% of total HCN channel subunits leaving the remaining 20% to HCN1 and HCN2 [12], [14]. HCN channels are activated by the hyperpolarization of the membrane potential, which allows both K^+ and Na^+ to pass through the pore. They are the molecular basis of the time-dependent inward current known as I_f in the heart or I_h in the nervous system [2]. Within the heart, HCN channels are primarily expressed in the sinoatrial node (SAN) region, the area responsible of the generation of spontaneous firing underlying rhythmic heartbeat [15]. In SAN myocytes, activation of HCN channels depolarizes the cell to the threshold of voltage-gated Ca^{++} channels activation and

eventually leads to an action potential firing [16], [17]. For this characteristic, HCN channels are also named pacemaker channels.

HCN channels similarly mediate pacemaker activity in the nervous system [2]. HCN channels can also stabilize the membrane resting potential of neurons [18]. In fact, they are activated at rest, leading to an inward sodium current that depolarizes the cell. This depolarization deactivates HCN channels, preventing too rapid firing [19]. Moreover, in neurons, HCN channels contribute to integrate electrical inputs by temporally and spatially summing the excitatory post synaptic potentials (EPSPs) to generate a single sensory output at the soma [20].

Given their crucial role in controlling cell excitability, mutations in HCN channels are related to several different types of cardiopathies and neuropathies [21], [22]. In the last two years I contributed to the functional characterization of some mutations found both in HCN1 and HCN4 in patients with both severe forms of early childhood epilepsy (HCN1) [5] and cardiac arrhythmias (HCN4) [9].

1.2 Biophysical properties of HCN current

Unique among the family of voltage-gated channels, HCN current activates upon membrane hyperpolarization. In a typical current trace elicited by HCN channel, two kinetic components can be distinguished upon activation: a minute instantaneous current which is fully activated within a few milliseconds, and a predominant slowly developing time-dependent component that reaches steady-state within seconds. Differently from most of the voltage-gated currents, HCN current does not display voltage-dependent inactivation in any of the mammalian isoforms (Fig.1).

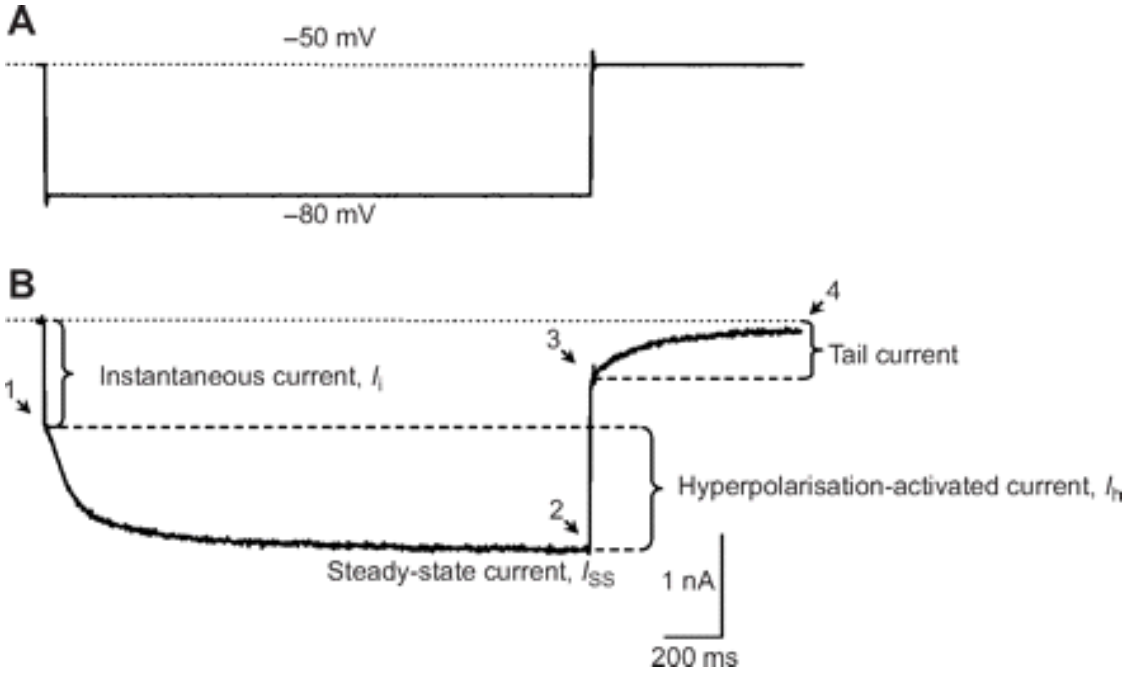

Figure 1: Biophysical proprieties of I_h current in neurons.
*Single step voltage protocol from –50 to –80 mV to -50mV (**A**) induced the current shown in (**B**). The amplitude of I_h is given by the difference between the instantaneous current at the beginning of the voltage step (I_i; 1) and the steady state current measured at the end of the pulse (I_{SS}; 2). After return to the reference potential, a falling tail current remains (3), which represents the time constant of channel-closing at the imposed membrane voltage in voltage-clamp mode. After complete deactivation, the current returned to resting values (4). Gerard et al 2012* [23].

The nature of the instantaneous current of HCN channels is currently subject of discussions. Both the presence and the amplitude of this component are variable in the different systems where the channels are expressed [24]. Some studies confer to this component characteristics resembling a small voltage-independent leakage current [25]. Others proposed that the instantaneous component is caused by a second pore that is found within an HCN channels subgroup that is not in equilibrium with the voltage gating population of the channels [26].

Concerning the steady-state component, its activation can be described by a single or double exponential function. The voltage dependence of activation is usually assessed by calculating the tail current activation curve, in which the amplitude of the tail current upon return to a fixed holding potential is plotted as a function of the preconditioning voltage step used to activate the current [2]. The activation curve is a typical sigmoid and describes the relative conductance of a population of channels at a given voltage; fitting with a Boltzmann function provides the half-maximal activation

("midpoint") potentials ($V_{1/2}$). The $V_{1/2}$ value represents the voltage at which 50% of the maximum achievable open probability has been reached [2] (Fig. 1.2).

Despite the high sequence similarity (80-90% identical), the HCN isoforms, when expressed as homotetramers, show quite distinct current kinetics and voltage dependence [27]. In particular, HCN1 has the fastest kinetic and the least negative threshold of activation [13]. Furthermore, it is also clear that cellular-specific environment can fine-tune HCN channel activity by means of auxiliary subunits, concentration of cellular factors, phosphatidylinositols etc. [1], [2].

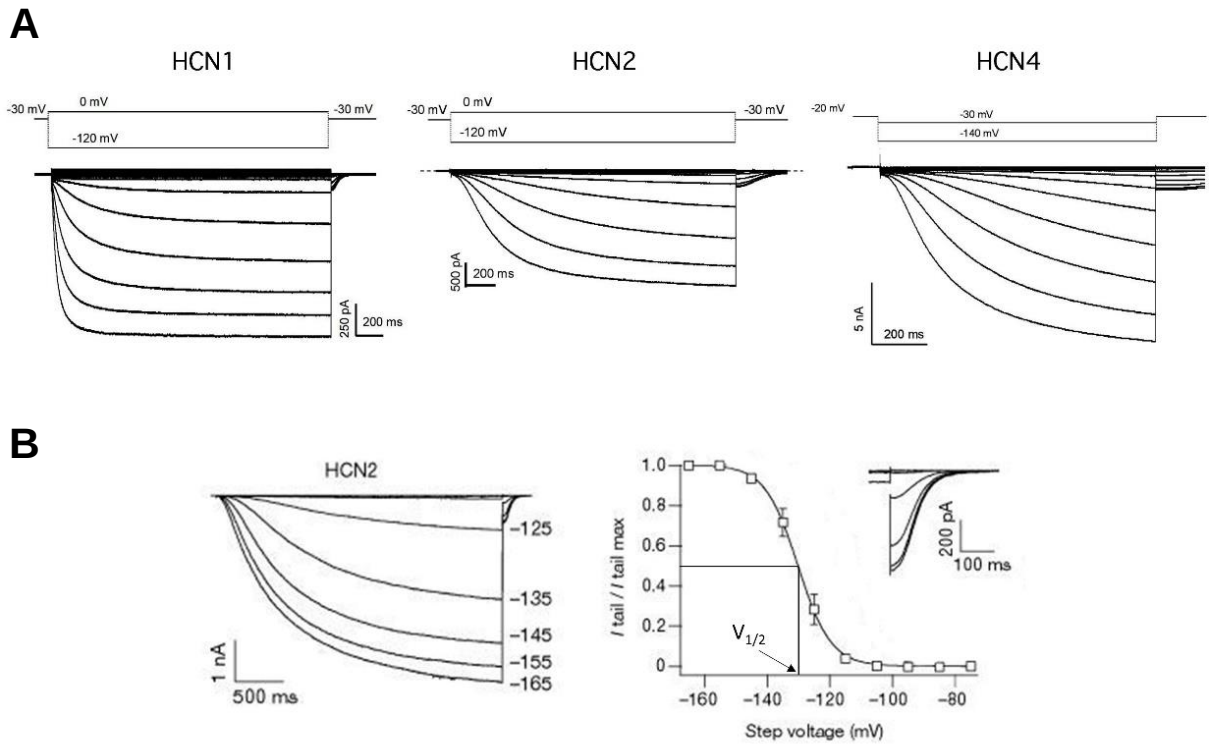

Figure 1.2: Biophysical proprieties of HCN homotetramers channel isoforms expressed in heterologous expression systems.
*(**A**), representative current traces elicited by HCN1 (left), HCN2 (centre) and HCN4 (right) using the indicated hyperpolarizing voltage step protocol. From the traces it is clearly visible the difference in the activation and deactivation kinetics (it is noted that HCN1 current reaches the saturation at more depolarized voltage compared to HCN2 and HCN4). (**B**), activation curve originated from normalized peak inward tail current amplitude, collected in the trace on the left, plotted as a function of voltage (right). Fitting of the sigmoidal curve provide the midpoint activation potential ($V_{1/2}$) indicated with the black arrow. Inset shows the tail current used to determine the activation curve. Modified from Wanger et al.*[28]

The current which permeates HCN pore is a mixed cation current that is carried by both K^+ and Na^+. The calculated ratio of the Na^+ to K^+ permeability of the channel (P_{Na}:P_K) ranges from 1:3 to 1:5 [1]. As a consequence, for example, the activation of I_h at resting membrane potentials results in an inward current carried mainly by Na^+, which depolarizes the membrane potentials. Both the current amplitude and the K^+: Na^+ permeability ratio are affected by the external K^+ concentration. Increased extracellular potassium concentrations result in an increased current amplitude as well as in a reduced selectivity for potassium over sodium [29]. HCN current is blocked by low concentration of Cesium (1-2 mM are sufficient to block 50% of the current), but is completely insensitive to external Barium, the most known blocker of inward rectifier potassium channel [29], [30]. Some evidences assign to HCN channels a small but significant permeability to divalent Ca^{++} ions, but the functional relevance of this feature remains still unknown [31], [32]. HCN single channel conductance has been found to be very small. There are few single-channel recordings of HCN channels; some of them revealed a single channel conductance in the range of 1pS [1].

1.3 Cyclic nucleotide regulation

HCN channels are activated by membrane hyperpolarization which is the main driving force able to open the pore; moreover, channel opening can be modulated by the direct binding of cyclic nucleotides to the intracellular cyclic nucleotide binding domain (CNBD) [33]. Binding of cAMP (3'-5'-cyclic adenosine monophosphate) or cGMP (3'-5'-cyclic guanosine monophosphate) at nanomolar concentration shifts the voltage-dependence gating of HCN channels to more depolarized potentials, accelerates the kinetics of activation and, in HCN2 only, increases the maximal conductance of the channel [19], [33]. Despite the high similarity (about 90% identical) of their CNBD regions, different isoforms have a distinct response to cAMP (Fig. 1.3), with HCN1 barely responding: in HCN1 the shift due to cAMP binding is only 3mV, while in HCN2 and HCN4 increases up to about 15-17mV [13], [34]. Similar is the effect evoked by the cGMP, but with much lower affinity [35].

In HCN2, this effect is associated with an increase in the maximal current [36], [37]. Taken together, these two effects could be explained with a model in which channel opening consists of a voltage-dependent activation step coupled to a voltage-independent opening step: cAMP binding enhances channel opening and shifts the voltage dependence of gating to more positive potentials by stabilizing the closed to open transition of the channel [38]; moreover, cAMP act also on the voltage-independent closed-open transition enhancing the maximal open probability at extreme hyperpolarized voltages, where voltage-dependent gating is already complete [36], [37].

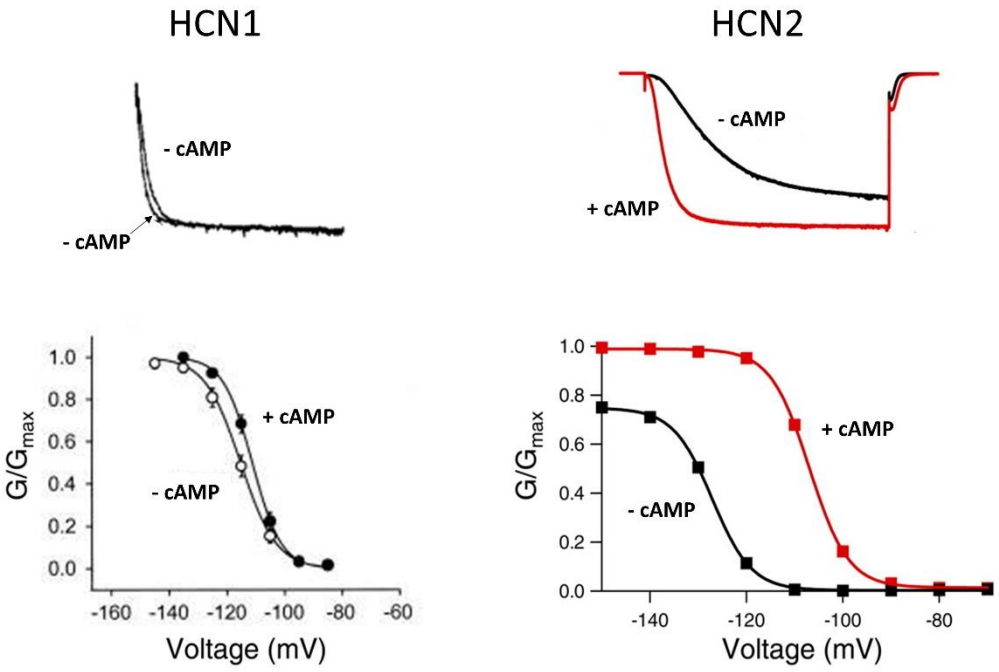

Figure 1.3: HCN1 and HCN2 are differently regulated by the binding of cAMP.
Currents elicited in response to single step potential of -135 mV (HCN1) and 120 mV (HCN2) in the presence and in the absence of cAMP are shown in the top panel. Activation curves of HCN1 and HCN2 channels recorded in inside-out configuration are shown in the bottom panel (left and right respectively). Cyclic nucleotide binding has a little effect on HCN1 kinetics as well as on the activation curve while it produces a more pronounced effect on both the speed of kinetics and the activation curve in HCN2 isoforms. It is noted the additional effect of cAMP biding on maximal tail current on HCN2 isoform (see the text).

The regulation of HCN channels by cAMP is relevant for the control of physiological processes. In the heart, cAMP contributes to both the speeding and the slowing of the heart rate in response to both β-adrenergic agonists (which raise levels of cAMP) and muscarinic acetylcholine receptor agonists (which reduce levels of cAMP). In the

nervous system neurotransmitters can influence firing rates by either increasing or decreasing cAMP levels that finally speeds the activation kinetics and maximal current levels of HCN channels [39] (Fig. 1.4).

A fine cAMP regulation is fundamental for the correct physiological contribution of HCN channels both in the heart and in nervous system. Recently, a single point mutation was found in the gene of hHCN4 channel in patients of a family which co-segregates with symptoms of Inappropriate Sinus Tachycardia (IST). Functional characterization of HCN4 channels carrying this mutation showed an increased cAMP sensitivity compared to the wild-type condition, supporting the importance of the cyclic nucleotide regulation of the I_f current in the heart [4].

Recent in-vivo studies have furthermore highlighted that I_h current elicited by HCN2 channels expressed in nociceptive neurons is predominantly responsible of inflammatory and neuropathic pain: modulating the action potential firing in these sensory neurons HCN channels are therefore able to control the pain perception [40], [41]. Among other consequences, the inflammatory processes activate signalling transduction pathways, which cause an increase of cAMP in pain-sensing neurons [42]. In-vitro studies carried-out in isolated DRG neurons related such increase in cAMP levels with the potentiation of HCN channels opening and consequently with the shift of the resting membrane potential to depolarized values, finally leading to an increased action potential firing caused by inflammation and nerve injury [40].

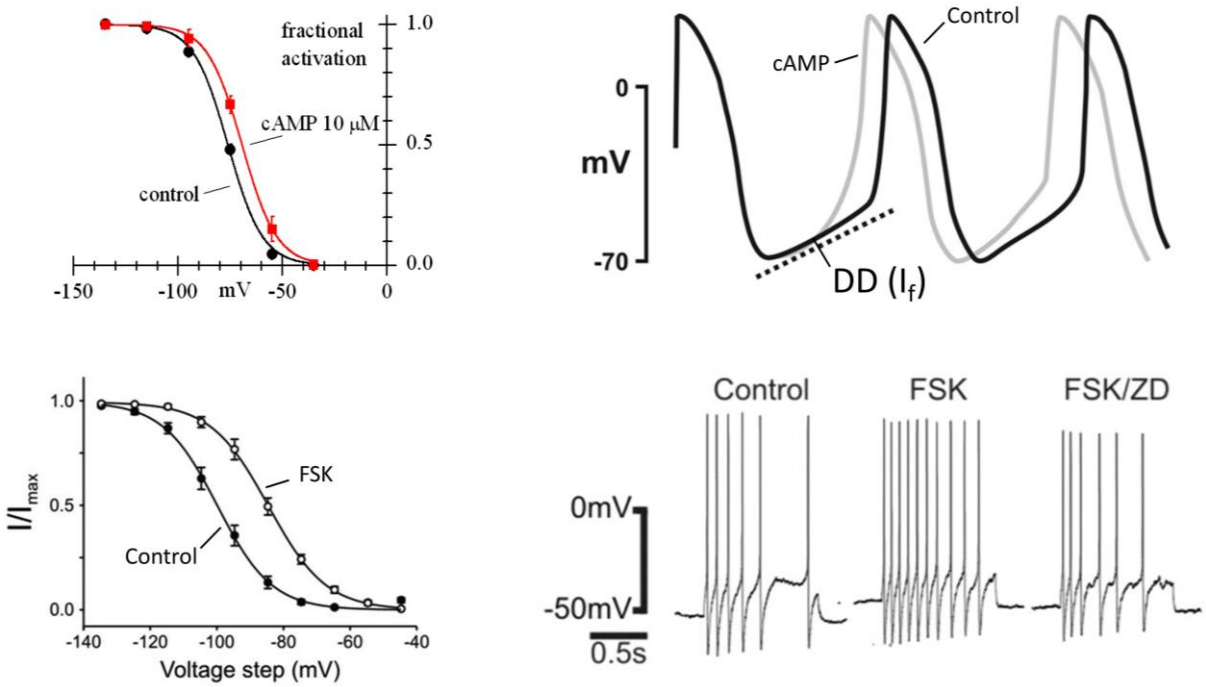

Figure 1.4: cAMP regulation of native I_f (top panel) and I_h (bottom panel) current.
Addition of 10μM of cAMP to sinoatrial node cardiomyocytes shifts the I_f $V_{1/2}$ toward more depolarized potentials (top, left) and speed up the spontaneous heart rate (top, right). DD indicates the diastolic depolarization phase of the cardiac pacemaker potential generated by the funny current. The change in the slope of DD phase induced by the cAMP (dot line) leads to the acceleration of the heart rate potential.
Voltage dependence of the I_h current in small DRG neurons is shifted by the application of forskolin (FSK, an activator of adenylate cyclase) which increases the cAMP levels (bottom, left). Action potential firing elicited by a constant pulse in small DRG neurons is enhanced by the application of FSK. Application of ZD (ZD7288, an HCN channels selective blocker) restored the firing rate to values comparable to the control confirming that the acceleration of the firing rate is HCN dependent (bottom, right). Modified from Wahl-Scott and Biel [10] *and from Emery et al.* [41].

1.4 HCN channel architecture

1.4.1 The transmembrane region

HCN channels belong to the superfamily of voltage-gated potassium (Kv) channels. As already postulated and recently confirmed by the high resolution Cryo-EM structure, each subunit of HCN channels is composed by six transmembrane segments (TM S1-S6): S5-S6 helices assemble in the center of the tetramer to form the pore region; instead, the first four helices (S1-S4) form the voltage sensor domain (VSD), that, in HCN channels is “not swapped” (Fig. 1.5). This means that, in contrast to voltage-gated potassium (Kv) and voltage-gated sodium and calcium (Nav and Cav) channels, each voltage sensor contacts the pore through amino acids from the same subunit [3].

The selectivity filter contains the sequence conserved in K^+ channels (GYG motif), but HCN channels are permeable to K^+ and Na^+ with a ratio of 4:1; moreover, they are blocked by Cs^+ and insensitive to Ba^{++}. The Cryo-EM structure [3] revealed that this difference could be due to a different angle of the side chain of the Tyrosine of GYG motif in HCN channels compared to K^+ channels. Due to this different conformation, the number of sites available for the binding with the K^+ ion is reduced from the canonical four of the K^+ channels [43] to two, allowing the flowing of some Na^+ ion.

The voltage sensor contains in TM S4 helix the positive charged residues responsible of its motion upon changes in membrane potential. Notably, HCN channels show an opposite voltage sensitivity compared to the other Kv channels. Several studies were conducted in order to describe the movement of the S4 upon hyperpolarization of the membrane potential. The current model was obtained by measuring the binding of methanethiosulfonate reagent (MTSET, cationic [2-(trimethylammonium) ethyl] methane thiosulfonate) to cysteine residues specifically inserted in different position of the S4 [44]. In this way it was possible to determine whether a given residue was accessible to extracellular or intracellular aqueous environment in a state-dependent manner. Using this approach, the Siegelbaum group suggested that, upon membrane potential changes , the S4 segment does not move “up and down” as in Kv channels; instead, they proposed that the N-terminal region of S4 is almost static, while the C-terminal region undergoes substantial changes in environment during

voltage-gating [44]. The extent of HCN channel S4 movements during gating is still a matter of debate [44]–[46]. The Cryo-EM structure shows the down state, inactive, conformation of the voltage sensor only, due to the fact that structural studies are conducted in the absence of membrane voltage (0 mV) [3]. Moreover, the structure of the transmembrane domain in the cAMP bound and unbound state appear identical in the Cryo-EM structure of HCN1, because this isoform is not responding to cAMP binding. This structure therefore cannot be used to identify the conformational changes induced by the binding of the cyclic nucleotide in other, more responsive, HCN isoforms.

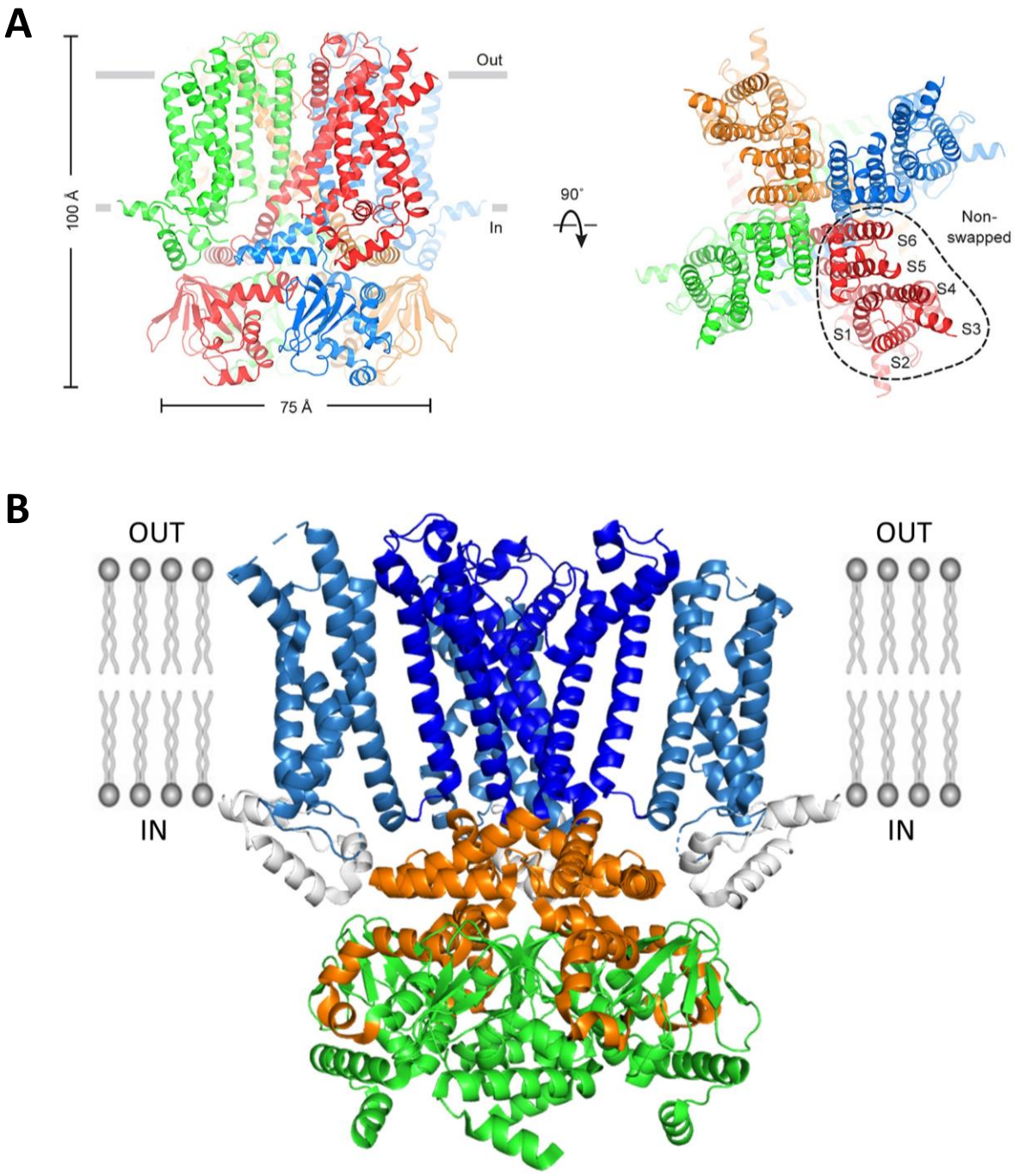

Figure 1.5: HCN1 channel architecture.
***A**, ribbon representation of the front view of the whole tetramer where each subunit is represented by a different colour (left). Grey bars delimit the thickness of the plasma membrane. Scale bars are indicative of the dimensions of the tetramer (left). The top view of the protein clearly shows the central ion conducting pore and the four "non-swapped voltage sensor domain" (right). **B,** the S5-S5 TM helices composing the pore region are highlighted in blue surrounded by the four transmembrane helices of the four voltage sensor domain (TM S1-S4) coloured in light blue. In orange and green are represented the C-linker region and the CNBD respectively (see next paragraph). For clarity, the voltage sensor closest to the viewer is not shown. Modified form Lee and MacKinnon* [3].

1.4.2 The C-terminal region

The cytosolic region of HCN channels is composed of two domains: the C-linker and the CNBD. At the interface between membrane and cytosol, the S6 helix bends giving rise to the six helices (from αA' to αF') interspersed by short loops composing the C-linker region that forms a tightly packed disc at the basis of the transmembrane region [3], connecting the last transmembrane segment to the underlying cyclic nucleotide binding domain (Fig. 1.5 and 1.6). The C-linker has a characteristic fold, in which the first two helices (A', B') form an antiparallel helix-turn-helix motif interacting with the helices C' and D' of the neighbouring subunit. These particular conformation has been equated to an “elbow on shoulder", and it involves interactions such as hydrogen bonds, hydrophobic interactions and salt bridges [3], [47]. Interestingly, despite the fact that the transmembrane helices are locked in the 0 mV conformation, overlapping of the cryo-EM structures in the cAMP bound and unbound state reveals subtle differences: in the bound conformation, the helices of the C-linker, undergoes slight rotation movements that are presumably associated with gate opening [3] (Fig. 1.6). This confirms the idea that the conformational changes initiated by cAMP in the CNBD propagate to the C-linker and to the transmembrane region, but the exact molecular events leading from initial cyclic nucleotide binding to facilitation of voltage-gated channel opening is still an open issue.

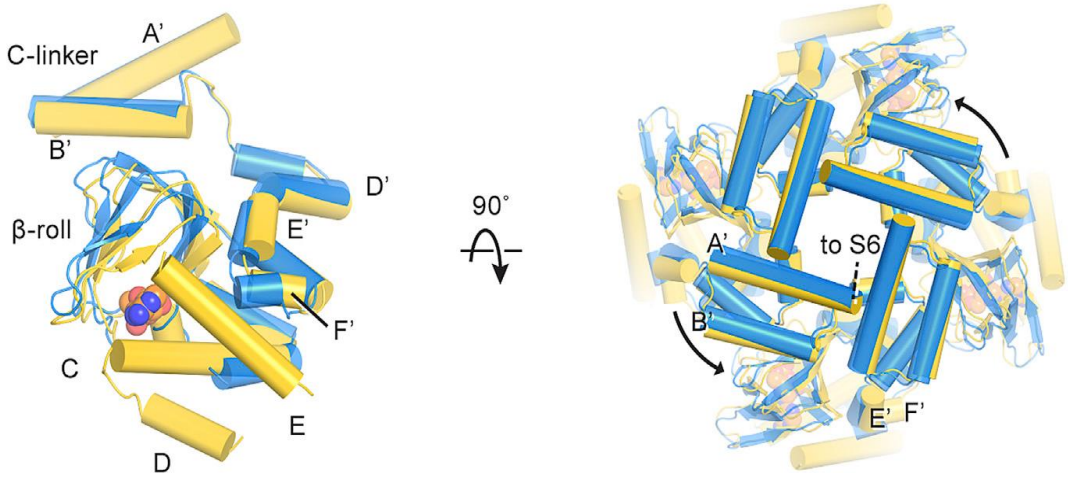

Figure 1.6: C-linker movements upon cAMP binding

Front view (left) and top view (right) of the C-linker-CNBD region in the cAMP bound (yellow) and cAMP unbound (blue) conformation. The binding of cAMP induces a rotation of the C-linker that is forced in the resting conformation by the position of the transmembrane helices. Lee and MacKinnon [3]

The CNBD is formed by four α-helices (αA, αB, αC, αP) and a β-roll in between the helices. The β-roll is composed by eight antiparallel β-strands (β1-β8) and contains the binding pocket of the cyclic nucleotides [47], [48]. The conformational changes induced by the binding of the cAMP are clearly visible in the Cryo-EM structure, and confirm previous observations of crystallographic and spectroscopic studies: binding of cAMP induces the folding of the P-helix, and causes the αA, αB, αC helices to approach the β-roll closing the pocket where the cyclic nucleotide is bound[49], [50] (Fig. 1.7). Notably, the conformational changes of αA helix causes an upward movement of the E', F' helixes of the C-linker (Fig. 1.6). This concerted movement of αA helix of CNBD and of E', F' helixes of the C-linker correspond to the mechanical transition of cAMP signalling from the CNBD to the C-linker [50]. Finally, the Cryo-EM structures of HCN1 highlight a new and unexpected conformational change caused by cAMP binding: the ligand induces the formation of two additional helices named αD and αE immediately after the αC helix of the CNBD [3].

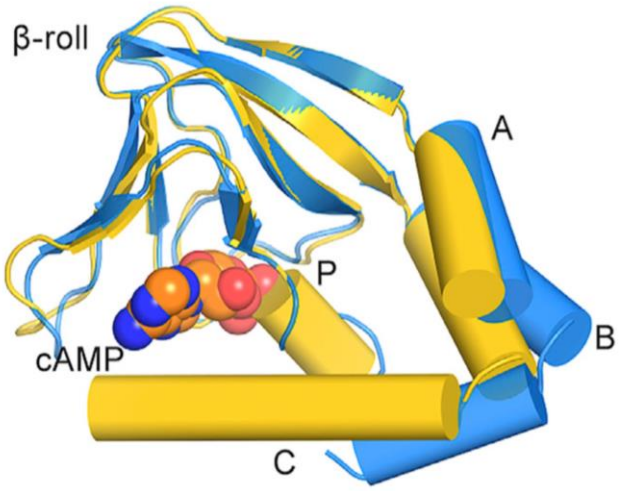

Figure 1.7: cAMP induces conformational changes in the CNBD.
Superimposition of the CNBD obtained from the Cryo-EM structure in the cAMP bound (yellow) and cAMP unbound conformation (blue). Alpha helices are shown as cylinders.

Basing the overlapping on the β-roll backbone the movements of the A', B' and C' helices as well as the folding of the P-helix are clearly visible. Lee and MacKinnon [3].

The binding of the cyclic nucleotide to the CNBD favours the tetramerization of the C-linker-CNBD C-terminal fragment, while monomeric and dimeric states prevail in the absence of the cyclic nucleotide [47]. Electrophysiological studies using tandem dimers or tetramers of HCN2 channels, where cAMP binding was allowed only in the selected subunits, showed that cAMP effect was stronger when functional CNBDs belonged to opposite subunits, thus determining that cAMP binding induces first a dimerization of CNBDs followed by a dimerization of these dimers into a tetramer [34].

In HCN channels the CNBD exerts a tonic inhibition on the channel pore, shifting the gating to more negative potentials [28]. This inhibition is released by ligand binding, with a consequent shift of the voltage dependence of activation described previously (see paragraph "The cyclic nucleotide regulation"). The inhibitory effect of CNBD that is removed by ligand binding is confirmed by electrophysiological data showing that the deletion of this domain causes the same effect of cAMP in facilitating channel opening [28].

1.4.3 The N-terminal region

The amino terminus of HCN channels include a region, about 45aa long, that is conserved among all isoforms (identity > than 90%). Using confocal imaging and patch-clamp electrophysiology on mHCN2 channel, Tran and collaborators have found that this isoform-conserved sequence (aa 131 to 182 in mHCN2 sequence) is required for plasma membrane localization of channel protein and expression of HCN2 currents [51]. Channels lacking of such region are retained in the intracellular compartments, such as the endoplasmic reticulum or the Golgi apparatus, suggesting that this conserved domain of the NH_2 terminus is important for subunit co-assembly and trafficking of pacemaker channels [51] (Fig. 1.8). Subsequent confocal localization studies in *X. laevis* rod photoreceptors found that the altered expression of N-terminus deleted channels is due to the presence of ER export signal in the isoform conserved region that is necessary for the correct forward trafficking of HCN1 to the plasma membrane [52].

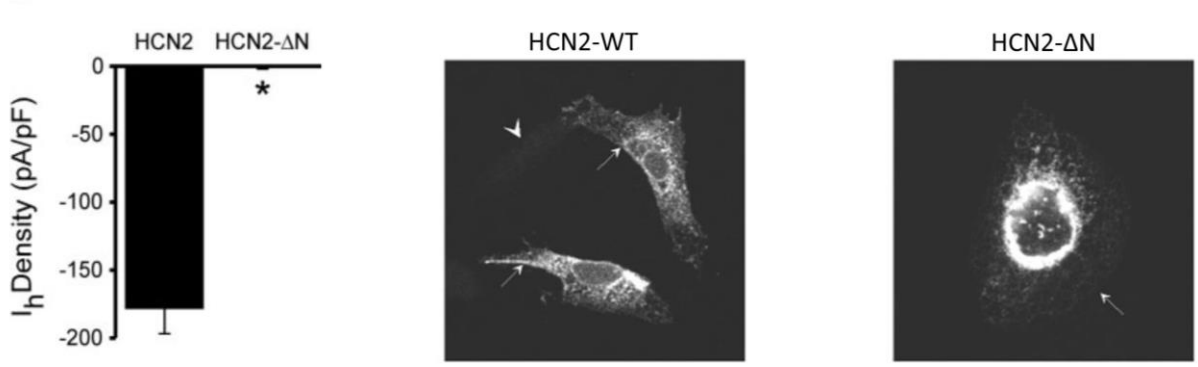

Figure 1.8: The N-terminal region is fundamental for functional expression of HCN2 channel. Deletion of the N-terminus comprising the conserved region causes the disappear of the current recorded in CHO cells transiently expressing the deleted channel (left). As confirmed by the confocal immunolocalization (centre and right) the channel is retained in intracellular compartments, with a pattern of expression consistent with a retention in endoplasmic reticulum or Golgi apparatus. The small arrows highlight the areas of the plasma membrane conspicuous for the presence of absence of fluorescence. Modified from Tran et al. [51].

Recently, a de novo gain of function mutation was found right in such region in the gene coding for hHCN1 channel in patients suffering of early infantile epileptic encephalopathy [8]. Functional characterization of the protein carrying this mutation (hHCN1 S100F) transiently expressed in Chinese hamster ovary (CHO) cells showed a significant shift of the $V_{1/2}$ of the activation curve coupled with an increase of the instantaneous component of the current [8]. This result suggests that in the N-terminal isoform conserved sequence of HCN channels there is something that is able to affect the gating proprieties of the channel. Patch-
clamp analysis on chimeric channels obtained swapping the N-terminus of mouse HCN1 with that of rabbit HCN4 showed no statistically difference in both the activation and deactivation kinetic nor in the activation curves [53], suggesting that the existence of a N-terminus mediated gating regulation (if any), could be a mechanism conserved among the isoforms.

A huge contribution to the understanding of the function of the N-terminal region comes from the hHCN1 structure. Lee and Mackinnon showed for the first time that the 45 residues preceding the S1 segment, which correspond to the isoform conserved region, give rise to three helices that form a domain nestled between the voltage sensor domain and the C-terminal cytoplasmic region. Since a domain with

these characteristics is unique of HCN channels it was called HCN domain [3] (Fig. 1.9).

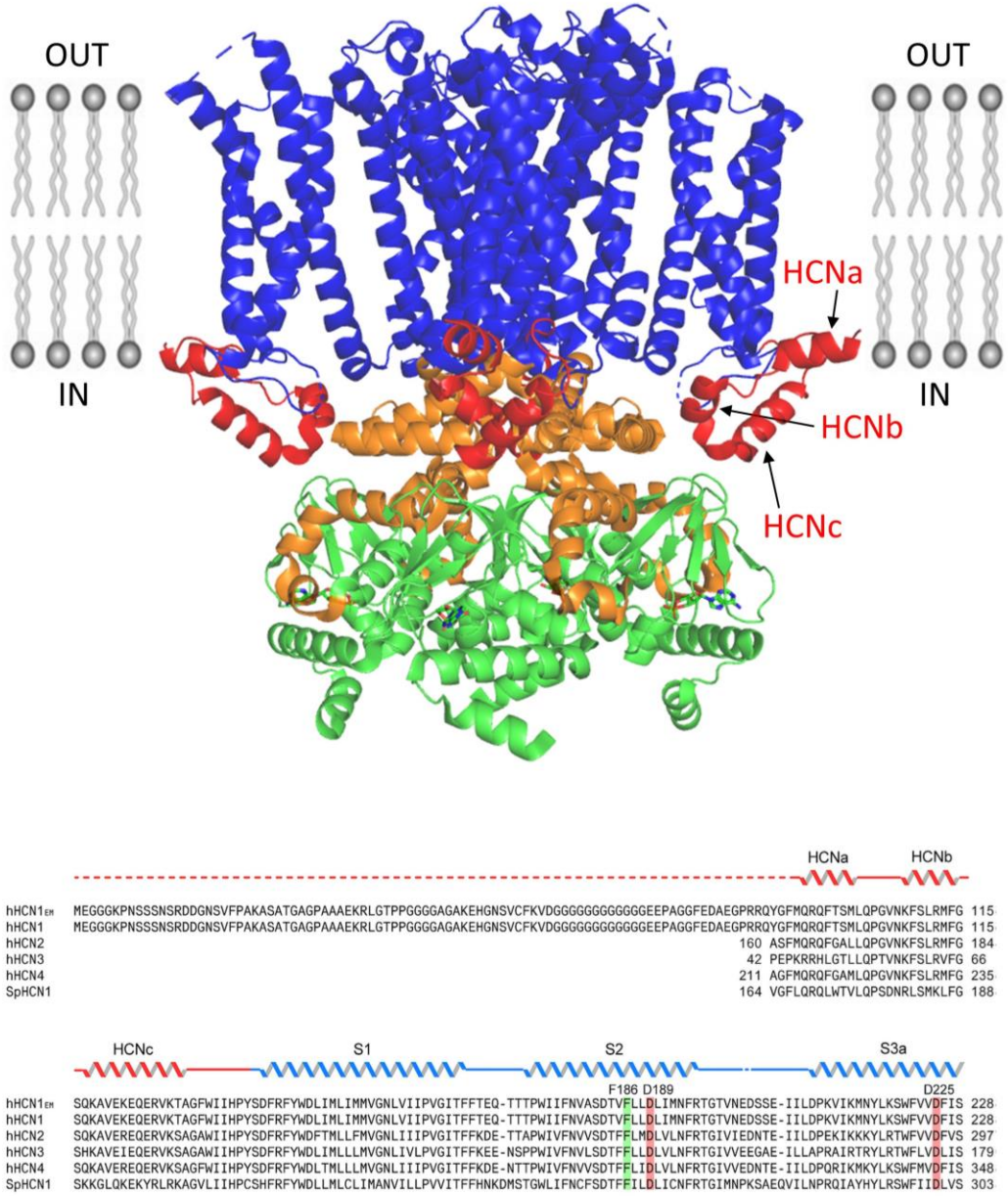

Figure 1.9: The new HCN domain.
Ribbon representation of the tetrameric protein structure. The HCN domain (coloured in red) is formed by the three helices (HCNa, HCNb, HCNc) indicated by the black arrows. It is noticed how the HCN domain is likely a bridge between the cytosolic C-terminal region and the transmembrane region. The HCN domain sequence correspond to the conserved region of the N-terminal domain of HCN channels. Modified from Lee and MacKinnon [3].

2 AIM OF THE WORK

The complexity of the gating mechanism of HCN channels, that includes the activation by the voltage and the regulation by the cAMP, make it difficult to produce a comprehensive model describing such dual modulation. A strong contribution to go further insight the details of this dual mechanism was made by Benndorf and collaborators who successfully applied patch-clamp fluorometry in combination with confocal microscopy and a fluorescent cAMP derivative (fcAMP) to simultaneously study ligand binding and voltage activation in HCN2 channels [6], [7]. The results they achieved with this technique showed that the voltage dependent activation gating in HCN2 channels is able to positively influence the ligand binding affinity. Moreover, they demonstrated that ligand binding affinity increases prior to channel opening by an hyperpolarizing voltage step. Indeed, they showed that values of voltages that are sufficient to an early opening of the pore are able to influence the affinity of the CNBD for the cyclic nucleotide; in other words, they demonstrated that a binding affinity increase precedes channel activation [6] (Fig. 2), concluding that the voltage sensor domain and at least one CNBD must be functionally coupled without involving the opening of the pore, but they did not identify the mediator of such coupling [6]. Furthermore, measuring steady-state and time-dependent ligand binding to functional but closed HCN2 channels they observed that the ligand binding evokes what it is called a conformational flip of all subunits in the channel; this “flip” is described as conformational changes that occur before, and separately from, the channel opening [7]. The authors proposed that this conformational changes could involve the transmembrane region, strengthening therefore the hypothesis of a direct coupling between the cAMP modulation and the voltage sensor domain without passing through the pore [7].

Despite the importance of having cryo-EM structures of both cAMP-bound and unliganded HCN1, these structures have indeed failed to provide significant insights into the mechanisms of ligand gating regulation, since all the transmembrane helixes movements are hampered by voltage sensor that is blocked in the 0 mV resting conformation. The results achieved by Benndorf and collaborators suggested that to fully explain the mechanism of the cAMP regulation, it must consider something that

directly connect the voltage sensor domain to the C-terminal region without engaging the pore. Therefore, since the newly discovered HCN domain occupies a position that is consistent with a connection between the voltage sensor domain and the C-linker-CBND region (Fig. 1.9), all the elements suggested us to explore the possibility that it is exactly the HCN domain the element that couples the cyclic nucleotide regulation with the voltage sensitivity and viceversa.

Thus, we started inspecting carefully the published hHCN1 structure with the aim to identify the residues involved in intra- and/or intersubunit interactions between the HCN domain and the rest of the protein. Combining rational structure-driven site-directed mutagenesis and patch-clamp electrophysiology, this project aims to gain more insight the mechanisms that allow these channels to be opened by voltage and simultaneously regulated by the binding of cyclic nucleotides. As previously discussed in the paragraph “The cyclic nucleotide regulation”, the binding of cAMP to HCN1 channel causes a minute shift. For this reason, the isoform used for the majority of the experiments showed in this work is the HCN2, which allowed a finest measurement of the cyclic nucleotide response. Moreover, basing on the results obtained on HCN2 the project aims also to perform some key experiments on HCN1 channel in order to confirm that the mechanism studied in this work are shared between the different isoform and/or if there are some difference between them.

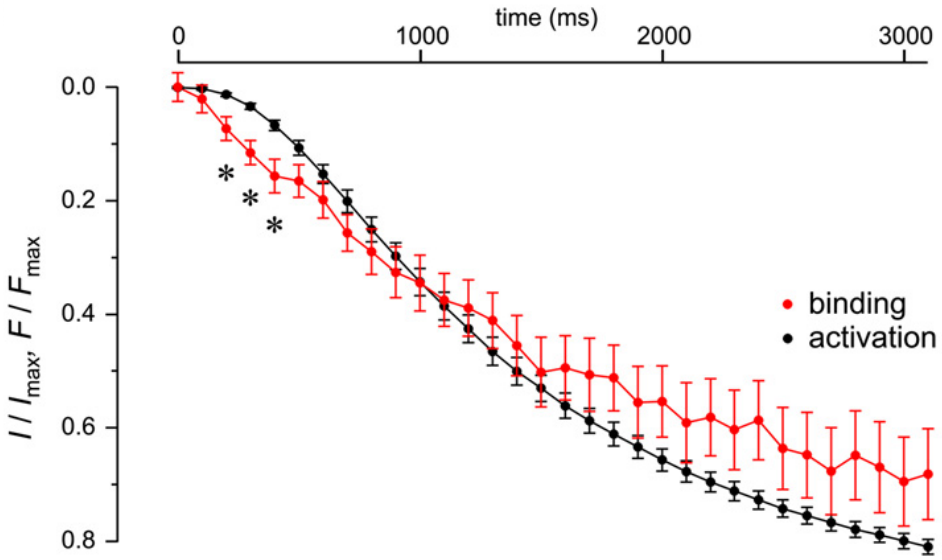

Figure 2: Early Activation-Induced Ligand Binding Significantly Precedes Current Activation. The normalized time dependent component of the current activation and the ligand binding at sub-saturating concentrations is shown in black and in red respectively. At early voltage activation, when the pore is at the first stages of the opening, the increase of the ligand

binding affinity is statistically higher, suggesting a coupling between voltage sensor domain and CNBD that does not involve the pore. From Kusch et al 2010 [6].

3 MATERIALS AND METHODS

Molecular biology

Human HCN1 (hHCN1, Xention Ltd., Cambridge, UK), mouse HCN2 (mHCN2, PMID: 11331358) and rabbit HCN4 (RbHCN4, PMID: 10212270) are the constructs used in this work. HCN genes are cloned in pcDNA3.1 (hHCN1) or in pCI (RbHCN4 and mHCN2) expression vectors. The construct used for immunolocalization experiments is the HCN2 of mouse in pEGFP-C1 vector (PMID: 21411649); in this plasmid a EGFP tag is fused in frame to the N-terminus of the protein of interest. Site-directed point mutations were introduced in hHCN1 and mHCN2 genes by the means of QuickChange Lightning ® (Agilent Technologies) kit and then confirmed by sequencing. This method is based on a PCR reaction, which requires specific primers to be designed to contain nucleotides mismatches that cause translation in a different aminoacid. Such primers were designed using QuickChange Primer Designer Tool (Agilent Technologies). The following formula was used for estimating the Tm of primers:

$$\mathrm{Tm} = 81.5 + 0.41(\%\mathrm{GC}) - (675/\mathrm{N}) - \%\,\mathrm{mismatch}$$

where N is the primer length in bases, %GC is the amount of Guanines (G) and Citosines (C) and % mismatch is the number of nucleotide mismatches.

The mixture for the PCR reaction was adjusted from the one suggested by the manufacturer:

10x Reagent Buffer	2,5 µl
dsDNA template	50 ng
Primer Forward	125 ng
Primer Reverse	125 ng
QuikSolution reagent	1,2 µl
dNTP mix	0,5 µl
QuikChange Lightning Enzyme	0,5

ddH_2O	To a final volume of 25 µl

The thermocycler was set with the parameters recommended by the manufacturer.
PCR products were incubated for 15min at 37°C with 1µl of *Dpn1* enzyme provided by QuickChange Lightning ® (Agilent Technologies) kit in order to degrade the dsDNA template.
The obtained PCR reactions were used to transform Stble2 competent cells. Stble2 competent cells derive from JM109 strain, which is specific for repeated sequences with the potential to recombine. Indeed, this strain carry both point mutations in endonuclease-coding gene *endA1* and recombinase-coding gene *recA* and deletions of locus *mcrAΔ* containing methylated DNA binding endonucleases genes (*mcrBC-hsdRMS-mrr*).
Media used for free growth and selective growth of *E.coli* strains were prepared as follow:

- LB (Luria-Bertani) Broth. Liquid medium used for free growth: 20g LB powder in 1L distilled water and autoclaved before usage. Desired antibiotics were added to make selective growth, according to the resistance carried by expression vectors.
- LB + Agar. Solid medium for selective growth: 20g LB powder and 15 g of Agar powder for 1L solution. Desired antibiotics were added to make selective growth, according to the resistance carried by expression vectors.

The transformation protocol used for Stbl2 competent cells is the following:

- a 50µl aliquot of competent cell was thawed in ice. When just thawed, 5ng of PCR product already treated with *DpnI* enzyme were added;
- incubated in ice for 30 minutes;
- heat shock at 42°C in a thermostatic bath for 25 seconds and then incubated in ice for 2 minutes
- added 500µl LB Broth without any antibiotic each 50µl of cells (10:1 ratio)
- pellet the culture, discarded the supernatant and resuspended the pellet
- plated on solid agar plates with the desired antibiotic and incubated overnight at 37°C

Exprep™ Plasmid SV kit (GeneAll) was used to extract and purify the plasmid DNA from competent cells according to the manufacturers recommended protocol

Cell culture and transfection

HEK293 cells were cultured in Dulbecco's modified Eagle's medium (Euroclone) supplemented with 10% fetal bovine serum (Euroclone), 1% Pen Strep (100 U/mL of penicillin and 100 µg/ml of streptomycin), and stored in a 37°C humidified incubator with 5% CO_2.

Every 2 or 3 days of the week cells were trypsinized and split to avoid the overgrowth. After 20-25 splits cells were discharged and a new fresh line was thawed to substitute the old one. Cells were grown in a $25mm^2$ flask and transferred in a 35m Petri dish (Sartstedt) the day before the transfection. When 70% confluent, HEK293 cells were transiently transfected with wild-type and/or mutant cDNA using Turbofect transfection reagent (Thermo Fisher) according to the manufacturers recommended protocol. For confocal imaging HEK293T cells were plated in the same way on 35mm glass Petri dishes and transfected with mHCN2 in pEGFP-C1 (wild-type and mutants).

Fluorescence analysis

30-72 hours after transfection, fluorescence analysis was carried out on living cells transfected with either the WT or mutant HCN2 channels; confocal microscopy was performed using a Nikon AZ-C2 (Nikon) microscope with a 60x objective, excitation was at 488 nm, and fluorescence was detected between 550 and 594 nm. Data was analyzed using ImageJ software (U.S. National Institutes of Health, Bethesda, MD, USA).

Electrophysiology on HEK cells and data analysis

For each 35 mm Petri dish 1 µg or 0,5 µg of the HCN-containing vector and 0.3 µg of GFP-containing plasmid (pmaxGFP, AmaxaBiosystems) were used. 30-72 hours after the transfection the cells were dispersed by trypsin treatment. Green fluorescent cells were selected for patch-clamp experiments at room temperature (about 25°C). Currents were recorded in whole-cells configuration with a Dagan 3900A (Degan, Minneapolis, MN, USA); data were digitized with an Axon Digidata 1322 A/D (Axon

Instruments, CA, USA) converter and analysed off-line with Axon pClamp9. Patch pipettes were fabricated from 1.5mm O.D. and 0.86 I.D. borosilicate glass capillaries (Sutter, Novato, CA, USA) with a P-97 Flaming/Brown Micropipette Puller (Sutter, Novato, CA, USA) and had resistances of 3–5MΩ

The pipettes were filled with a solution containing: 10 mM NaCl, 130 mM KCl, 1 mM egtazic acid (EGTA), 0.5 mM $MgCl_2$, 2 mM ATP (Mg salt) and 5 mM HEPES–KOH buffer (pH 7.4). The extracellular bath solution contained 110 mM NaCl, 30 mM KCl, 1.8 mM $CaCl_2$, 0.5 mM $MgCl_2$ and 5 mM HEPES–KOH buffer (pH 7.4). Where indicated, different volumes of Adenosine 3′,5′-cyclic monophosphate (cAMP, Sigma-Aldrich) were added to the pipette solution from a previously prepared stock solution in order to obtain different concentrations. The stock solution was prepared solving the powder in milliQ water in order to obtain a final concentration of 100mM and adjusting the PH to 7. Single-use aliquots were made and stored at -20°C until the day of the experiment.

The HCN domain peptide (sHD) (MQRQFTSMLQPGVNKFSLRMFGSQKAVEKEQERVKTAG) was synthetized and lyophilized by the peptide synthesis service of Tema Ricerca. The lyophilized protein was dissolved in milliQ water in order to obtain a stock concentration of 2,5 mM and divided in single-use aliquots stored at -80°C. The day of the experiment the solved peptide was thawed and added to the pipette solution at the final concentration indicated in the text.

For channel activation, hyperpolarizing steps of variable duration, sufficient to reach steady-state activation at all voltages, were applied from a holding potential and current tails were measured upon return to a fixed voltage (-40mV for all the isoforms). The duration and the number of the steps used to activate the channels was adjusted for the different HCN isoform. Whole-cell measurements of HCN channels were performed using the following voltage clamp protocol depending on the HCN isoform measured: for HCN1, holding potential was –30 mV (1 s), with steps from –20 mV to –120 mV (10 mV interval, 3.5 s) and tail currents recorded at –40 mV (3 s); for HCN2, holding potential was –30 mV (1 s), with steps from –40 mV to –130 mV (10 mV interval, 5 s) and tail currents recorded at −40 mV (5 s); for HCN4, holding potential was –30 mV (1 s), steps from –30 mV to –165 mV (15 mV interval, 4.5 s) and tail currents were recorded at −40 mV (5 s).Only cells in which a 1 GΩ

seal or better was achieved were kept for analysis. Patch-clamp currents were acquired with a sampling rate of 5 KHz and lowpass filter of 0.5 kHz. Currents were normalized to cell capacitance. Neither series resistance compensation nor leak correction were applied.

Mean activation curves were obtained by fitting maximal tail current amplitude, plotted against the voltage step applied, with the Boltzmann equation

$$I_t = I_t(max)/(1+\exp(V-V_{1/2})/k$$

where I_t is the current amplitude of the tail current recorded for a given prepulse and $I_t(max)$ is the maximum current amplitude of the tail current, V is the voltage of the prepulse, $V_{1/2}$ is the half-activation voltage and k is the slope factor in mV using Originpro software (Originlab, Northampton, MA, USA).

The dose-response curves data were analysed by fitting the Hill equation, as follows:

$$S/Smax = 1/[1+(k_{1/2}/ [ligand])n]$$

where S is the shift in $V_{1/2}$, $k_{1/2}$ is the half-maximal concentration, and n is the Hill factor using Originpro software (Originlab, Northampton, MA, USA)

All the measurements were performed at room temperature. Mean $V_{1/2}$ values derived by the Boltzmann fitting were compared using one-way ANOVA followed by Fisher's test or using Student's t-test as indicated in the figure legends. Significance level was set to p=0. 05. All data are presented as mean ± S.E.M.

SAN isolation and electrophysiology

SAN pacemaker cells were isolated from adult mice hearts. Mice were killed by cervical dislocation under general anaesthesia consisting of 0.01 mg/g xylazine (2% Rompun; Bayer AG), 0.1 mg/g ketamine (Imalgène; Merial) and 0.04 mg/g of Na-pentobarbital (Euthanasol VET, Laboratoire TVM, Lempdes, France); thus, beating hearts were quickly removed. The SAN region was excised in Tyrode's solution containing: 140 mM NaCl, 5.4 mM KCl, 1.8 mM $CaCl_2$, 1 mM $MgCl_2$, 1 mM Hepes-NaOH (pH = 7.4), and 5.5 mM D-glucose and some incisions were made to help the subcessive enzymatic digestion. The tissue was transferred into a 'low-Ca^{2+}-low-

Mg^{2+}' solution containing: 140 mM NaCl; 5.4 mM KCl, 0.5 mM $MgCl_2$, 0.2 mM $CaCl_2$, 1.2 mM KH_2PO_4, 50 mM taurine, 5.5 mM D-glucose, 1 mg/ml bovine serum albumin (BSA), 5 mM Hepes-NaOH (pH = 6.9) and digested by adding Liberase TH (0.15 mg/ml, Roche Diagnostics GmbH, Mannheim, Germany), elastase (1.9 U/ml, Worthington, Lakewood). Digestion was carried out for a variable time of 10–15 min at 37°C. Tissue strips were then washed and transferred into a modified 'Kraftbrühe' (KB) medium containing: 70 mM L-glutamic acid, 20 mM KCl, 80 mM KOH, (±) 10 mM D- b-OH-butyric acid; 10 mM KH_2PO_4, 10 mM taurine, 1 mg/ml BSA and 10 mM Hepes-KOH (pH = 7.4). Single SAN cells were isolated by mechanical dissociation in KB solution for 30–50 s (or until all the pieces of tissue were disintegrated). Cellular automaticity was recovered by re-adapting the cells to a physiological extracellular Ca^{2+} concentration by addition of a solution containing: 10 mM NaCl, 1.8 mM $CaCl_2$ and normal Tyrode solution containing BSA (1 mg/ml). The final storage solution contained: 100 mM NaCl, 35 mM KCl, 1.3 mM $CaCl_2$, 0.7 mM $MgCl_2$, 14 mM L-glutamic acid, (±) 2 mM D-b-OH-butyric acid, 2 mM KH_2PO_4, 2 mM taurine, 1 mg/ml BSA, (pH = 7.4). Electrophysiological experiments were performed after 1-2h from the isolation. For electrophysiological recording, SAN cells in the storage solution were transferred in custom-made recording plexiglas chambers with glass bottoms for proper cell attachment and mounted on the stage of an inverted microscope (Olympus IX71) and perfused with normal Tyrode solution. The recording temperature was 37°C. Multiclamp 700B (Axon Instruments Inc., Foster USA) patch-clamp amplifier coupled to an Axon Digidata 1550B (Axon Instruments, CA, USA). Pipette were fabricated using microelectrode puller (Zeitz-Instruments Vertriebs GmbH, Martinsried, Germany). Electrodes had a resistance of about 3 MΩ. I_f was recorded under standard whole-cell configuration during perfusion of standard Tyrode's containing 2 mM $BaCl_2$ to block I_{K1}. Patch-clamp pipettes were filled with an intracellular control solution containing: 130 mM KCl, 10 mM NaCl, 1 mM EGTA, 0.5 mM $MgCl_2$ and 5 mM HEPES (pH 7.2). sHD was added as described previously. I_f current was elicited by using a using the following voltage clamp protocol: holding potential was -35 mV (100 ms), with steps from -135 mV to -35 mV (10 mV interval, 1700 ms) and tail currents recorded at +5 mV (200 ms); Mean activation curves were obtained by fitting maximal tail current amplitude, plotted against the voltage step

applied, with the Boltzmann equation described previously. Statistical comparisons were made as described in the previous paragraph.

4 RESULTS AND DISCUSSION

4.1 Putative HCN domain interactions with the voltage sensor domain and the C-terminus

In order to test the hypothesis that the HCN domain is the element that mechanically connects the movements of the C-LINKER/CNBD to the voltage sensor domain (VSD), we carefully inspected the human (hHCN1) structure (PDB_ID: 5U6O [3]) searching for interactions among these domains.

The HCN domain contacts the VSD in the membrane by means of hydrophobic interactions that pinch the VSD from two sides, the side of S1-S2-S3 and the side of S4 transmembrane (TM) helices. We have renamed these two hydrophobic interactions “first” and “second”, respectively. In the cytosol, the HCN domain interacts with the C-linker and the CNBD by means of salt bridges (Figure 4).

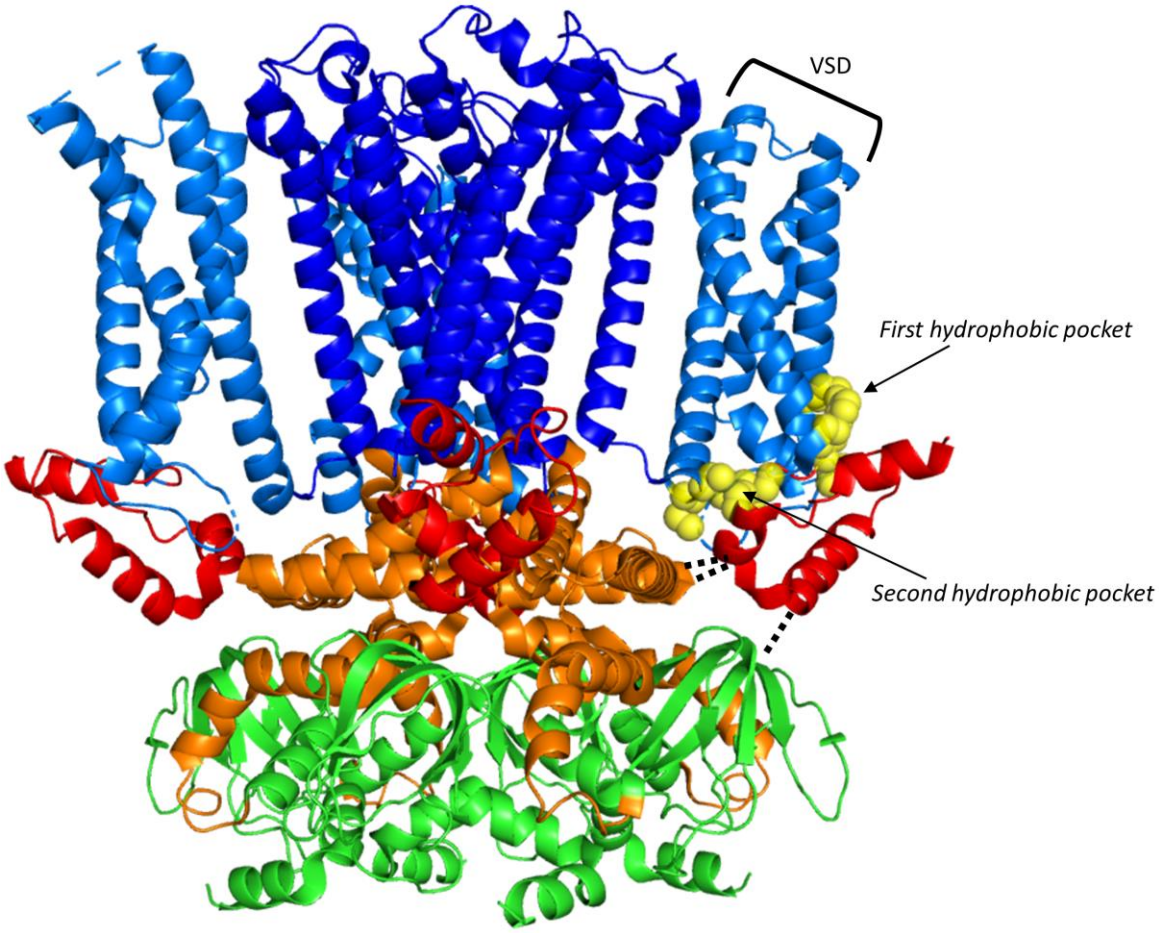

Figure 4: Ribbon representation of the apo-hHCN1 structure. The helices composing the pore region (S5-S6) are highlighted in blue. The four transmembrane helices forming the voltage sensor domain (from S1 to S4) are coloured in light blue. In orange and green are represented the C-linker region and the CNBD respectively. HCN domain is coloured in red. Yellow spheres represent the van der Waals surface of the side chains of the residues engaging intra-subunit hydrophobic interactions that connect the HCN domain with the VSD. Black arrows point the two different found hydrophobic pockets. Dashed black lines schematically represent the putative inter-subunit electrostatic interactions that connects the HCN domain to the C-linker/CNBD region. For clarity, the voltage sensor closest to the viewer is not shown.

The first hydrophobic interaction occurs by means of the Isoleucine 135 of the loop connecting the HCN domain to the beginning of TM S1. This side chain inserts in the membrane inside a hydrophobic pocket formed by residues belonging to the TM S1, S2 of the VSD: F140, M191 (Fig 4.1-A and -B).

Preceding I135 residue, there is a second Isoleucine, 134. Its sidechain points parallel to the membrane towards the S2-S3 loop that contains a stretch of hydrophobic residues: I206, I207 and L208 (Fig 4.1-A and -C).

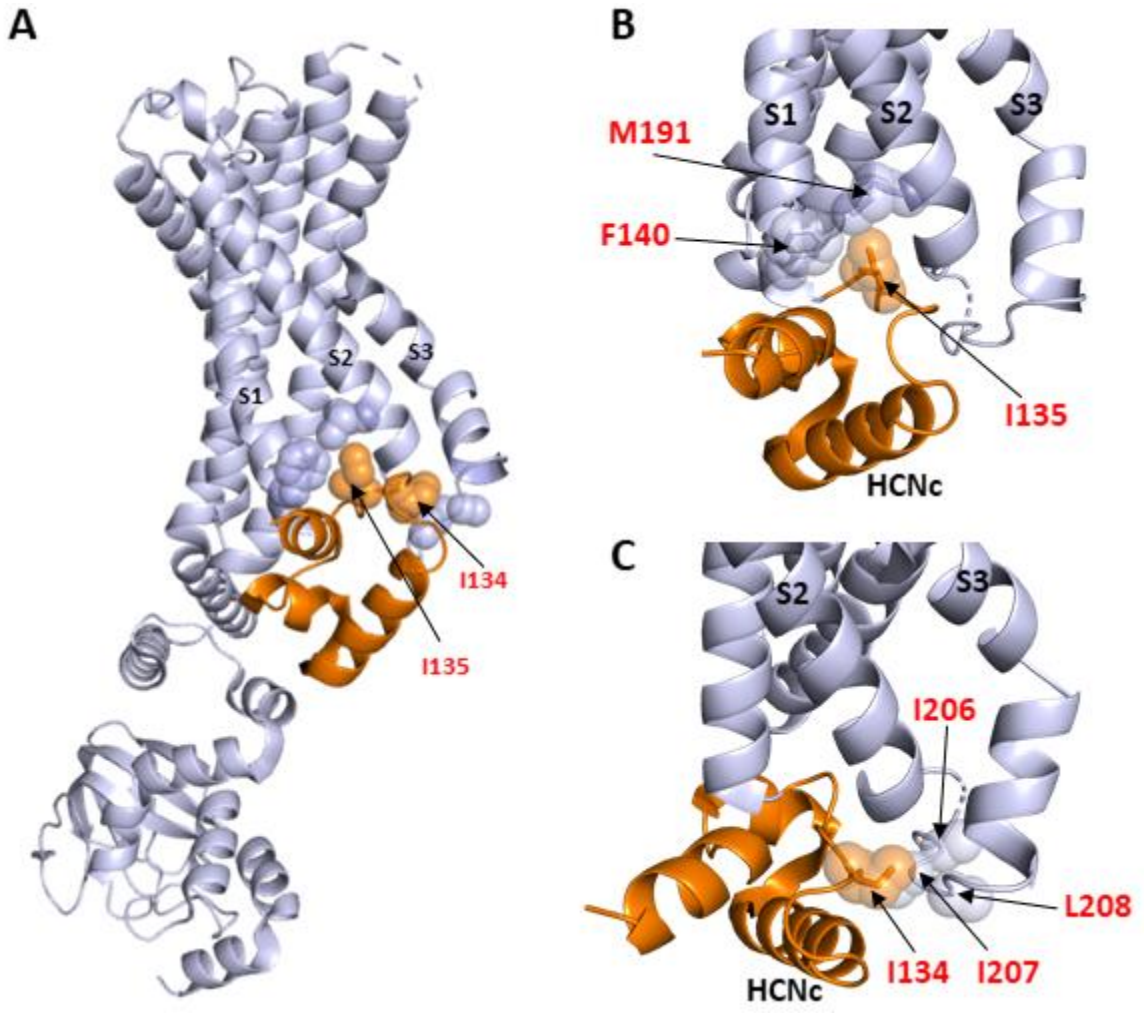

Figure 4.1: Structure of the first hydrophobic pocket. ***A****, ribbon representation of one of the four subunits of hHCN1 tetramer (from apo-structure). HCN domain is shown in orange. Spheres represent the Van der Waals surface occupied by the residues engaging intra-subunit hydrophobic interactions. I134 and I135 residues belonging to the loop connecting the HCN domain to the voltage sensor are indicated by the black arrows.* ***B-C****, two differently oriented views of the region comprising the hydrophobic pockets: the side chain of the amino acids involved in the hydrophobic interactions are shown as sticks. Corresponding Van der Waals spheres have the same colour code. In panel C, the side chain of the residues I206, I207, and L208 are not assigned because of the low resolution of the structure in this region; for these residues the Van der Waals spheres represent the surface occupied by the atoms of the main chain. Numbers refers to hHCN1 sequence.*

The second hydrophobic interaction is formed by Phenylalanine 151 residue that inserts its sidechain deeply inside a second hydrophobic pocket that is formed by residues I284 and M287, belonging to the TM S4 of VSD, and Y138 that connects the HCN domain to the TM S1 (Fig. 4.2).

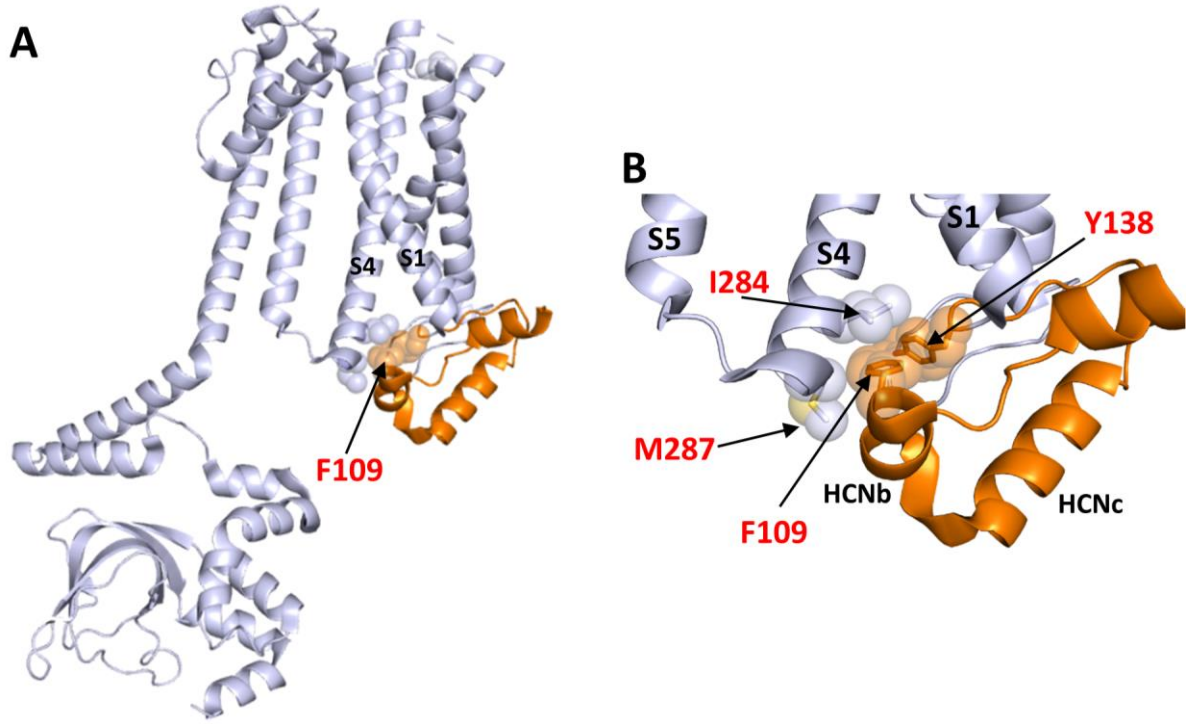

*Figure 4.2: **A**, ribbon representation of one of the four subunits of hHCN1 tetramer (from apo-structure). HCN domain is shown in orange. Spheres represent the Van der Waals surface occupied by the residues engaging intra-subunit hydrophobic interactions. F109 residue is indicated by the black arrow. **B**, Blow-up of the structure in A. The side chain of the amino acids involved in the hydrophobic interactions are shown as sticks depicted with the same colour of the sourcing main chain. Corresponding Van der Waals spheres have the same colour code. Numbers refers to hHCN1 sequence.*

In the cytosol, we found that HCN domain contacts the C-liker of both the adjacent and opposite subunit by mean of two electrostatic interactions. Concerning the contact with the adjacent subunit we identified a putative salt-bridge interaction between the amino group ($NH2^+$) of R112 residue of the HCN domain and the carboxyl group (COO^-) of E436 residue on the B' helix of the C-linker belonging to the adjacent subunit; the measured distance between the two functional groups is 3,3 Å (Fig. 4.3-A and -C). The other salt bridge interaction occurs between the main chain carbonyl group (CO^-) of M113 residue on the HCN domain and the ammonium group ($NH3^+$) of K422 residue on the A' helix of the C-linker of the opposite subunit (Fig. 4.3-B and -C); the measured distance between the two functional groups is 3 Å.

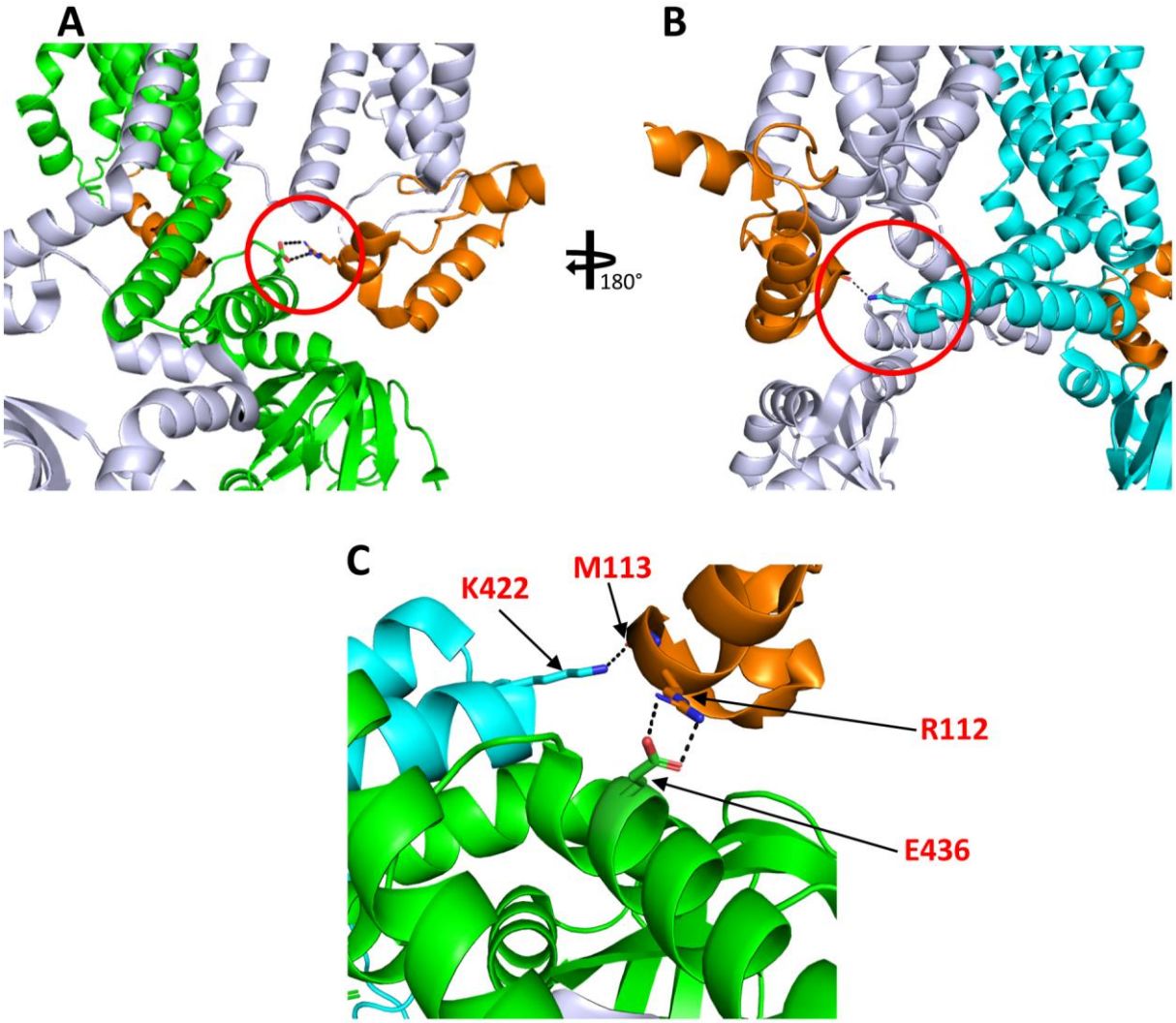

Figure 4.3: Electrostatic interactions between the HCN domain and the C-linker.
***A**, ribbon representation of two adjacent subunits (coloured in grey or in green) of hHCN1 tetramer. HCN domain is shown in orange. The putative salt bridge interaction is circled in red. **B,** ribbon representation of two opposite subunits (coloured in grey or in light blue) of hHCN1 tetramer. HCN domain is shown in orange. The putative salt bridge interaction is circled in red. **C,** Detailed view of the two salt bridge interactions between the HCN domain (orange) and the C-linker of the adjacent (green) and opposite subunit (blue). The side chains of the residues engaging the electrostatic interactions are shown as sticks. Numbers refer to hHCN1 aminoacid sequence.*

Inspecting the HCNb helix of the HCN domain, we found the side chain of a positive charged residue (K118) pointing in the direction of the beta-strand of the CNBD, in proximity of a negative Aspartic acid residue (D536) located in the β4-β5 loop (Fig. 4.4). However, the low-resolution of the CNBD structure in such region precludes the assignment of the side chains of several residues, making it impossible to know the exact position of the side chain of D536 as well as its distance from K108. Basing on

this indication and considering the relatively small distance (5.6 Å) between the ammonium group of the K118 residue and the α-carbon of the main chain of D536 residue, we did not exclude the possibility of an electrostatic attraction between the HCN domain and the CNBD.

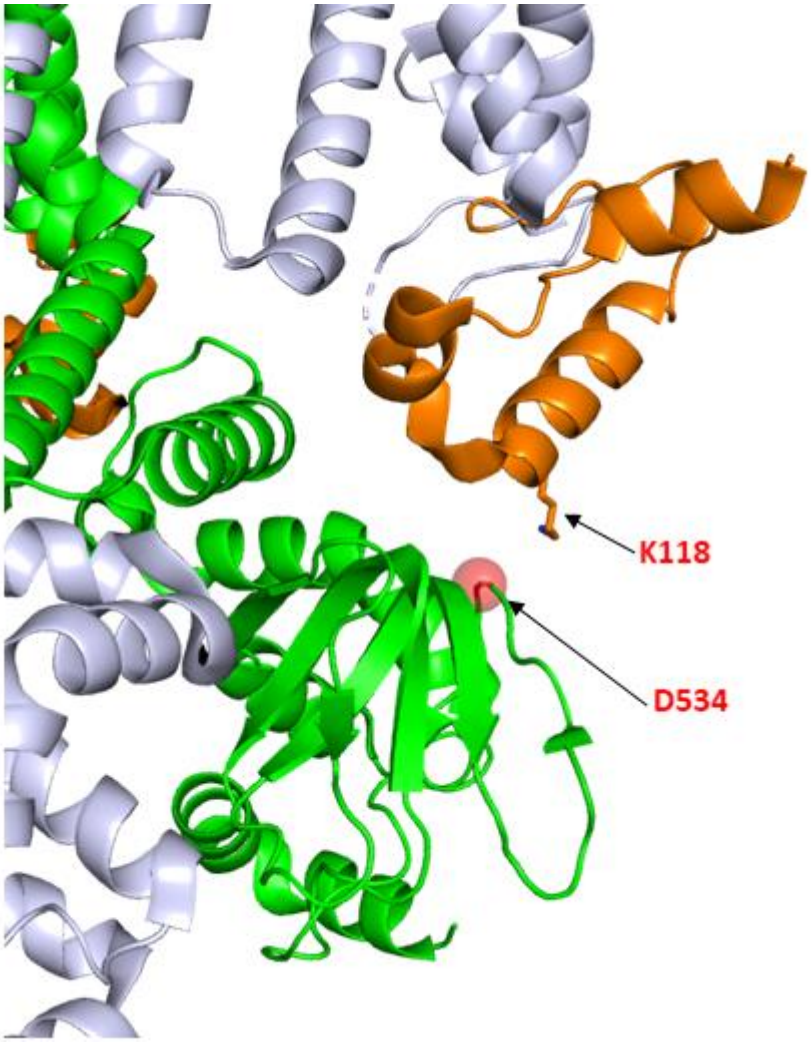

Figure 4.4: Putative electrostatic interaction between the HCN domain and the CNBD. Detailed view of two adjacent subunits of hHCN1 tetramer coloured in grey or in green. HCN domain is shown in orange. Side chain of K118 residue of the HCN domain is represented as stick. Red Van der Waals volume of α-carbon of D534 main chain is shown to indicate the position of the D534 residue on CNBD, speculated to be the possible partner of an electrostatic interaction with the K118 residue. Numbers refer to hHCN1 aminoacid sequence.

The alignment of human HCN1 (hHCN1) and mouse HCN2 (mHCN2) aminoacid sequences confirmed that all residues involved in the above described interactions are conserved among the two isoforms. The only (conservative) difference is the

M191 residue of HCN1 identified in the first hydrophobic pocket that in HCN2 corresponds to a Leucine (L234, see next paragraph). We therefore decided to perform the study based on mutational analysis of the crucial amino acids on mHCN2. This has two advantages: 1- working with HCN2 provides an easy assay for cAMP effect; 2- it extends our working hypothesis to another HCN isoform, providing evidence for a general gating scheme in HCNs. To this second aim, key mutations found to have an effect in HCN2 were studied also in hHCN1.

All mutant channels were transiently expressed in mammalian HEK293T cells and their currents analysed by patch-clamp technique in whole-cell configuration (Fig. 4.5). From the current measurements we estimated the half activation voltage ($V_{1/2}$), both in the absence and in the presence of cAMP. These values were obtained from the fitting of the Boltzmann function to the channel activation curve (Fig 4.5). The cAMP effect was not tested on HCN1, because, in HEK293T cells, the $V_{1/2}$ of this isoform is already fully shifted to the right by the endogenous cAMP and does not respond further (Fig 4.5-B). In order to help the reader to distinguish between hHCN1 or mHCN2 residues numbering, in the structural representations of the interactions showed in the following paragraphs, the residues involved in the interactions will be labelled with a double numbering: labels coloured in red and in black will refer to hHCN1 or mHCN2 sequences respectively.

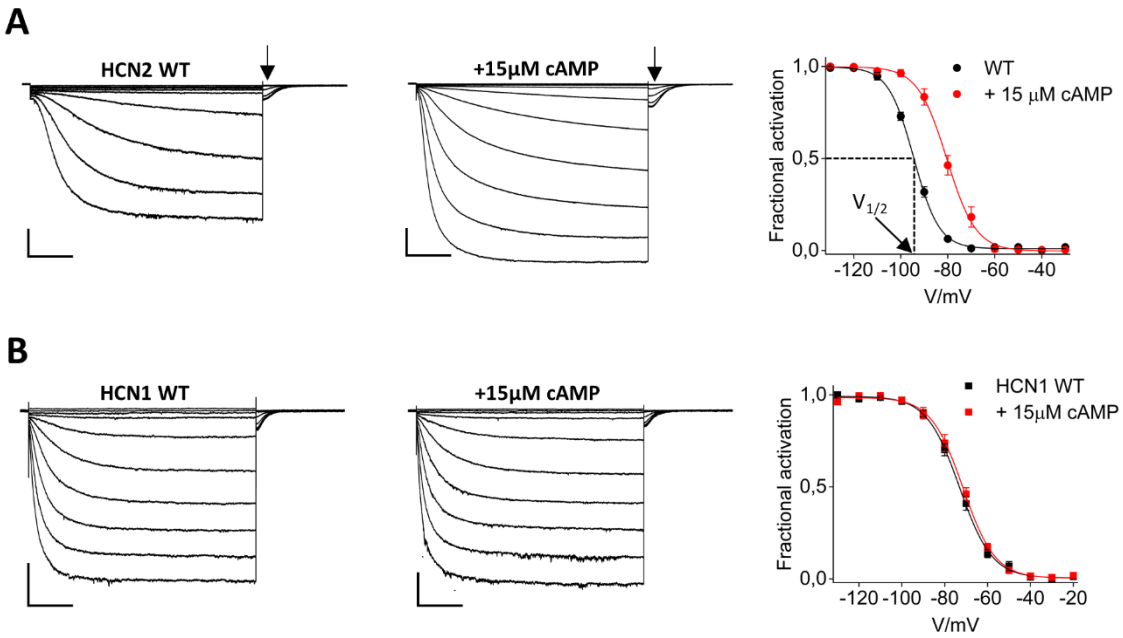

Figure 4.5: Whole-cell patch-clamp recordings of mHCN2 and hHCN1 channels. Representative currents recorded from HEK293T cells transiently expressing mHCN2 WT channel in absence (A, left) and in presence (B, centre) of cAMP or hHCN1 WT in absence (B, left) and in presence (B, centre) of cAMP. Tail currents (indicated by black arrows) are plotted against the voltage to obtain the activation curve shown in right panels. Lines show data fit to a Boltzmann function providing half activation potential (mean $V_{1/2}$ ± SEM) and inverse slope factor (mean k ± SEM) values as follow: $V_{1/2}$ = -94,4 ± 0,7 mV, k = 5,5 ± 0,1 (HCN2 wild-type); $V_{1/2}$ = -80,5 ± 0,6mV§, k = 6,1 ± 0,3 (HCN2 wild-type + 15µM cAMP); $V_{1/2}$ = -71,4 ± 0,8 mV, k = 8 ± 0,9 (HCN1 wild-type); $V_{1/2}$ = -71,5 ± 0,5 mV, k = 7,5 ± 0,6 (HCN1 wild-type+ 15µM cAMP). §p<0.05 by Student's T-test compared to untreated condition.

4.2 The first hydrophobic interaction controls channel's voltage-dependence

In the hHCN1 structure, the S1 and S2 transmembrane helixes pull away from each other, allowing the formation of a pocket occupied by the hydrophobic side chains of I135 (from HCN domain loop), F140 (from S1) and M191 (from S2), that, all together, contribute to the formation of the hydrophobic plug shown in Figures 4.6-A. An additional hydrophobic residue, I134 (from HCN domain loop) is found below the membrane and its side chain is pointing towards the cytosolic S2-S3 loop (Fig 4.6-B). The low-resolution of the structure in this region precludes the assignment of the side chains of the amino acids of the S2-S3 loop. Nevertheless, given the position of the backbone of the protein in the loop region, we speculated that the aliphatic side chains of the residues I207, L208 may contribute to form another hydrophobic plug

located at the interface between the HCN domain loop and the base of S2 and S3 segments.

As previously mentioned, the hydrophobic nature of the residues involved in these interactions is conserved between HCN1 and HCN2 channels, allowing us to work indistinctly on both the isoforms.

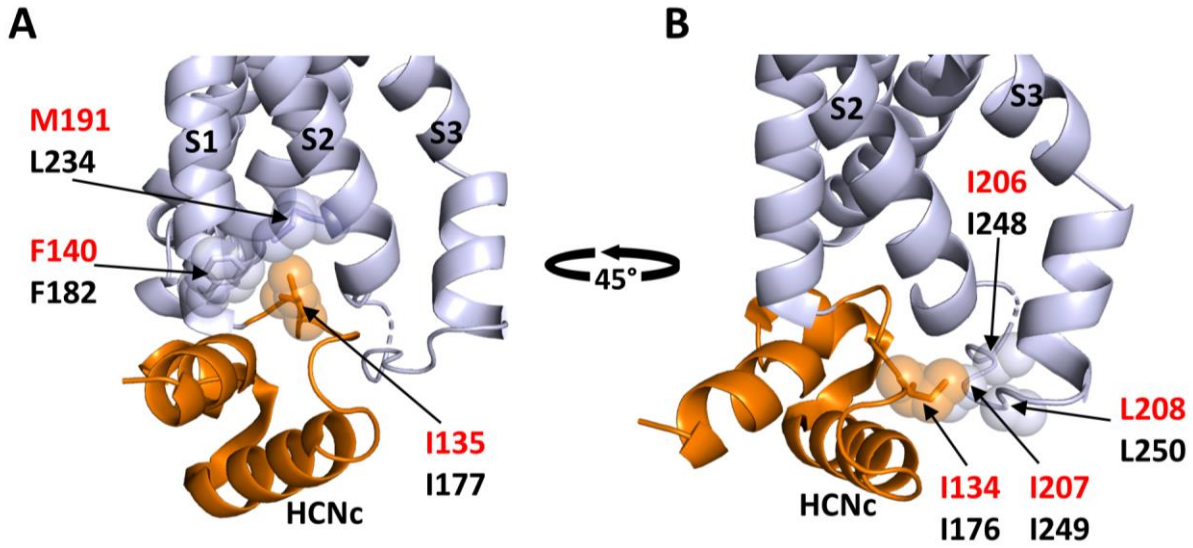

Figure 4.6: Detailed views of the "first hydrophobic pocket".
***A**, Hydrophobic interactions of I135 residue; the side chain of the amino are shown as sticks depicted with the same colour of the sourcing main chain. Corresponding Van der Waals spheres have the same colour code. **B**, the side chain of the residues I134 point towards the S2-S3 loop region, rich in hydrophobic residues. I207, L208, V212 and I213 are not assigned because of the low resolution of the structure in this region; for these residues the Van der Waals spheres represent the surface occupied by the atoms of the main chain. Numbers referring to hHCN1 or mHCN2 aminoacid sequence are coloured in red or black respectively.*

In order to evaluate the functional relevance of these hydrophobic interactions we started substituting the I177 residue of HCN2 channel (corresponding to I135 of hHCN1) with a negatively charged aminoacid (D, aspartic acid), with the idea to disturb the hydrophobic pocket and consequently to disconnect the putative link between the HCN domain with the voltage sensor domain. The I177D mutant channel was co-transfected with GFP protein in HEK293T cells and patch-clamp experiments were performed either after 24 or 48 hours from the transfection on GFP positive cells. In both cases, in all the tested cells (n=13), we did not record any HCN-like current (Fig 4.7-B). There are several explanations for the disappearance of the current in the cells expressing I177D mutant: i) a strong decrease in the number of functional channels in the plasma membrane; ii) a reduction of the single channel

conductance; iii) a huge shift of the voltage dependence towards negative potentials. Since the latter two possibilities are difficult to be experimentally verified, we decided to test the first hypothesis by examining the subcellular localization of HCN2 I177D mutant and comparing it with that of wild type channel. For this purpose, we used a HCN2 wild-type or I177D channel carrying a GFP fluorescent tag fused to the first aminoacid of the N-terminus. The confocal images showed that while HEK293T cells expressing the wild-type channel displayed a fluorescent labelling on the cell surface, the fluorescence of the cells transfected with I177D protein is mainly localized in the perinuclear region, resembling the patter of expression that was found by Tran and collaborators in the absence of the entire N-terminus of HCN2 [51] (Fig 4.8). These results indicate that this hydrophobic region is probably crucial for the proper folding of the protein and consequently for its trafficking to the plasma membrane. Therefore, we first substituted the I177 residue with a Valine and then with an Alanine with the idea to keep the hydrophobicity of the residue in position 177 but reducing at the same time its length. In this way we expected to cause a milder destabilization of the hydrophobic pocket, mild enough to allow the trafficking of the channel to the plasma membrane. The results of the patch-clamp experiments show that the currents elicited by the HCN2 I177V (n=6) and I177A (n=18) channels (Fig 4.7-D and -E), as well as their gating proprieties (Fig. 4.7-F) are indistinguishable from those of wild-type channel. Since the negative charged residue was not tolerated and the hydrophobicity of the side chains of both the Valine and the Alanine residues seemed to be sufficient to keep the full integrity of the pocket, we substituted the I177 with a Glycine, an aminoacid that does not have any side chain. Similarly to I177D mutant, the cells expressing HCN2 I177G channel did not show any HCN like current (n=18) (Fig 4.7-C) suggesting that the presence of a hydrophobic residue in position 177 is necessary for the proper conformation of the hydrophobic pocket, whose integrity is probably fundamental for the trafficking of the channel to the plasma membrane.

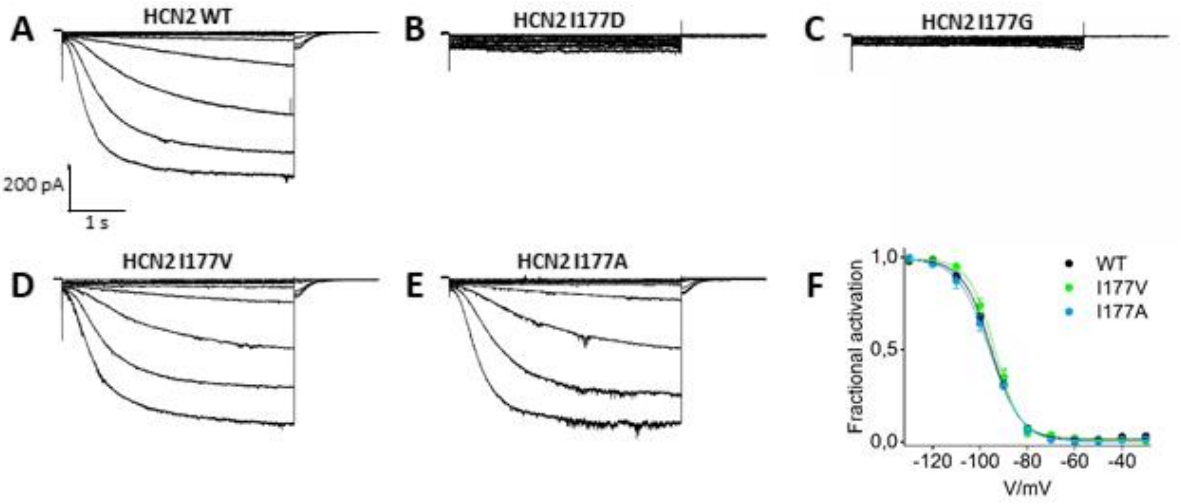

Figure 4.7: Patch-clamp recordings of mHCN2 I177 tested variants.
***A-E**, Representative whole-cell currents recorded from HEK293T cells transiently expressing wild-type, I177D, I177G, I177V or I177A mouse HCN2 channels as indicated. The protocol used for the recordings is described in material and methods. **F**, mean tail current activation curves of wild-type (black), I177V (green) and I177A (cyan) mutant channels. Lines show data fit to a Boltzmann function providing half activation potential (mean $V_{1/2}$ ± SEM) and inverse slope factor (mean k ± SEM) values as follow: $V_{1/2}$ = - 95,3 ± 0,5 mV, k = 6 ± 0,5 (wild-type); $V_{1/2}$ = -93,8 ± 0,6 mV, k = 5,5 ± 0,5 (I177V); $V_{1/2}$ = -96,0 ± 0,6 mV, k = 6,7 ± 0,6 (I177A). $V_{1/2}$ values are not statistically different from wild-type mHCN2 (One-way ANOVA with Fisher's test).*

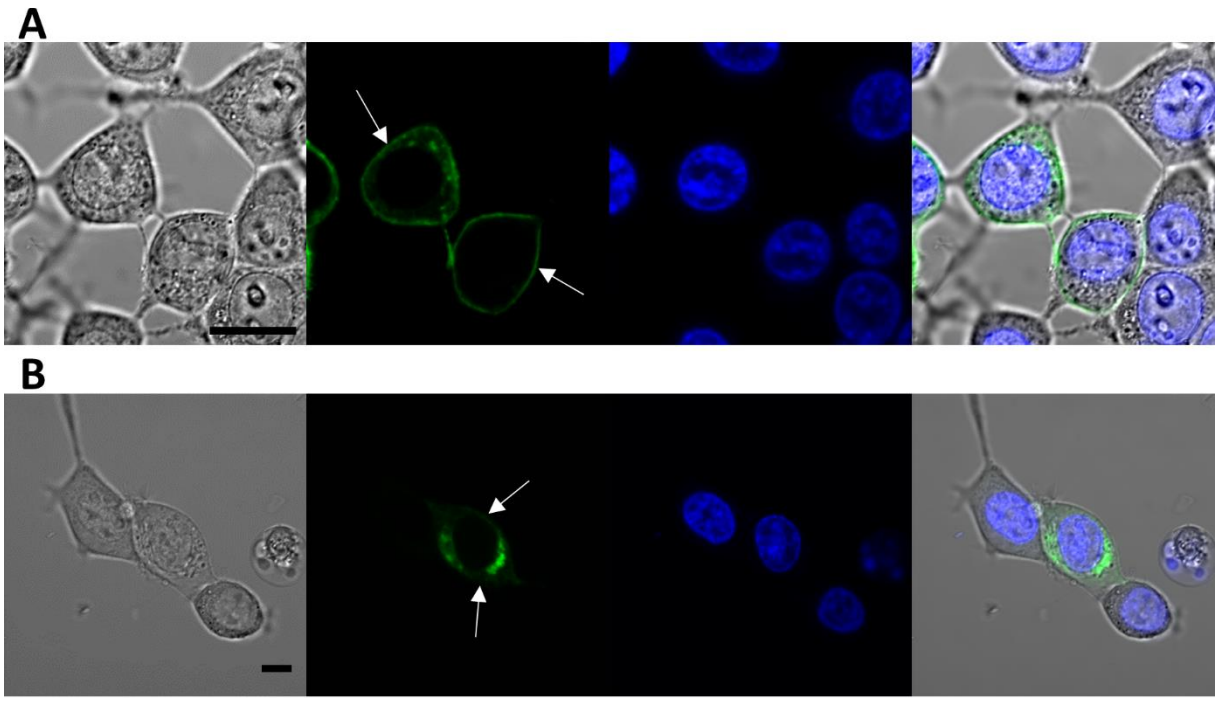

Figure 4.8: Cellular localization of WT HCN2 and I177D mutant.
*Confocal images of HEK293T cells transfected with GFP-HCN2 wild-type channel (**A**) or GFP-HCN2 I177D (**B**) mutant channel. Fluorescence images show GPF fused to the N-terminus of HCN2 channel (green) and Hoechst staining of nuclei (blue). The right panel is a*

merge of the three channels. The white arrows point to regions of the plasma membrane conspicuous for the presence or absence of fluorescence. Calibration bar: 100µm.

The key substitutions of I177 residue of HCN2 were tested in human HCN1 channel in order to verify that the effect is conserved between the two isoforms. Mutant channels were co-expressed with GFP protein in HEK293T cells and patch-clamp experiments were performed after both 24 and 48 hours from the transfection. Human HCN1 channels carrying the I135V mutation (corresponding to I177V of HCN2) generated a current that was indistinguishable from the wild-type (Fig 4.9-B and -D), while introducing a Glycine we could not detect any HCN-current (Fig 4.9-C); hence, these results support the results obtained on HCN2, i.e. that in position 135 of hHCN1 protein (corresponding to 177 of HCN2 sequence) is required a hydrophobic side chain that, ensuring the correct integrity of the pocket, probably allows the proper trafficking of the channel to the plasma membrane.

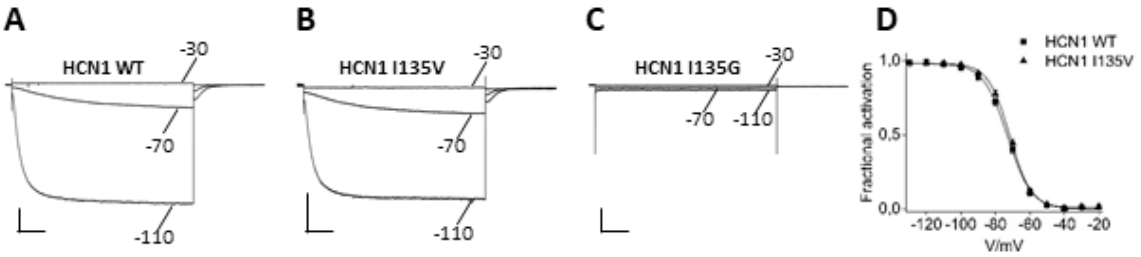

Figure 4.9: Patch-clamp recordings of hHCN1 I135 tested variants.
***A-C**, Representative whole-cell currents recorded, at the selected voltages, from HEK293T cells transiently expressing wild-type, I135V or I135G human HCN1 channels. The protocol used for the recording is described in material and methods. Scale bars represent 200pA and 1sec. **D**, Mean tail current activation curves of wild-type (black triangles) and I135V (black squares) mutant channels. Lines show data fit to a Boltzmann function providing half activation potential (mean $V_{1/2}$ ± SEM) and inverse slope factor (mean k ± SEM) values as follow: $V_{1/2}$ = - 72,9 ± 0,5 mV, k = 6,9 ± 0,3 (wild-type); $V_{1/2}$ = -71,7 ± 0,4 mV, k = 6,2 ± 0,3 (I135V). $V_{1/2}$ values are not statistically different from wild-type hHCN1 (Student's T-test).*

We then focused on the study of the functional role of the hydrophobic plug placed at the base of S2 and S3 transmembrane helixes, that hosts the side chain of the I134 residue of the HCN domain loop (Fig 4.6-B). Initially, we substituted the I176 residue of mHCN2 (corresponding to I134 in hHCN1) with an Aspartic acid, to disrupt the hydrophobic interaction. None of the tested HEK293T cells expressing HCN2 I176D channel showed an HCN-like current (n=10) (Fig. 4.10-C), indicating that, also in this position, any charged residue is probably not tolerated. As we did for I177 amino

acid, we proceeded substituting the I176 amino acid with residues having a hydrophobic side chain but a lower length than Isoleucine. When the Isoleucine was substituted with a Valine (HCN2 I176V), the channel generated a current indistinguishable from those of the wild-type (n=5) (Fig 4.10-B and -D). Further decreasing the length of the side chain of the residue 176 using an Alanine, we achieved the purpose of disturbing the hydrophobic interaction without losing channel activity at the plasma membrane. A functional HCN current was measured in only the 28% of cells expressing HCN2 I176A channel (n=10 to 35). In the cells where we could record an HCN current, we observed a drastic loss of the time dependent component accompanied by an increase of the instantaneous component of the current (Fig. 4.10-E); these strong effects precluded the analysis of the tail currents making it impossible to get an activation curve of the mutant channel. Application of extracellular cesium (2mM CsCl), a known HCN channel blocker, inhibited the HCN2 I176A current almost completely, confirming that the observed instantaneous component is generated by the mutant channel (Fig. 4.10-E).

To functionally demonstrate that the substitution of the I176 residue with an Alanine effectively altered the hydrophobic plug located at the base of the S2 and S3 helixes, we mutated one of the residues on the S2-S3 loop that we thought could be part of the putative hydrophobic plug. To this aim we selected L250 residue of mHCN2 channel and we mutated it into an Alanine. When transfected in HEK293T cells, the HCN2 L250A mutant showed about the same decrease in the expression levels of I176A mutant (only about 22% of the tested cells were expressing an HCN current); moreover, the current generated by the L250A mutant is characterized by a loss of the time dependent component accompanied by an increase of the instantaneous component (Fig 4.10-F), both features that are in common with the I176A mutant. Also, his current was totally blocked by cesium (Fig 4.10-F).

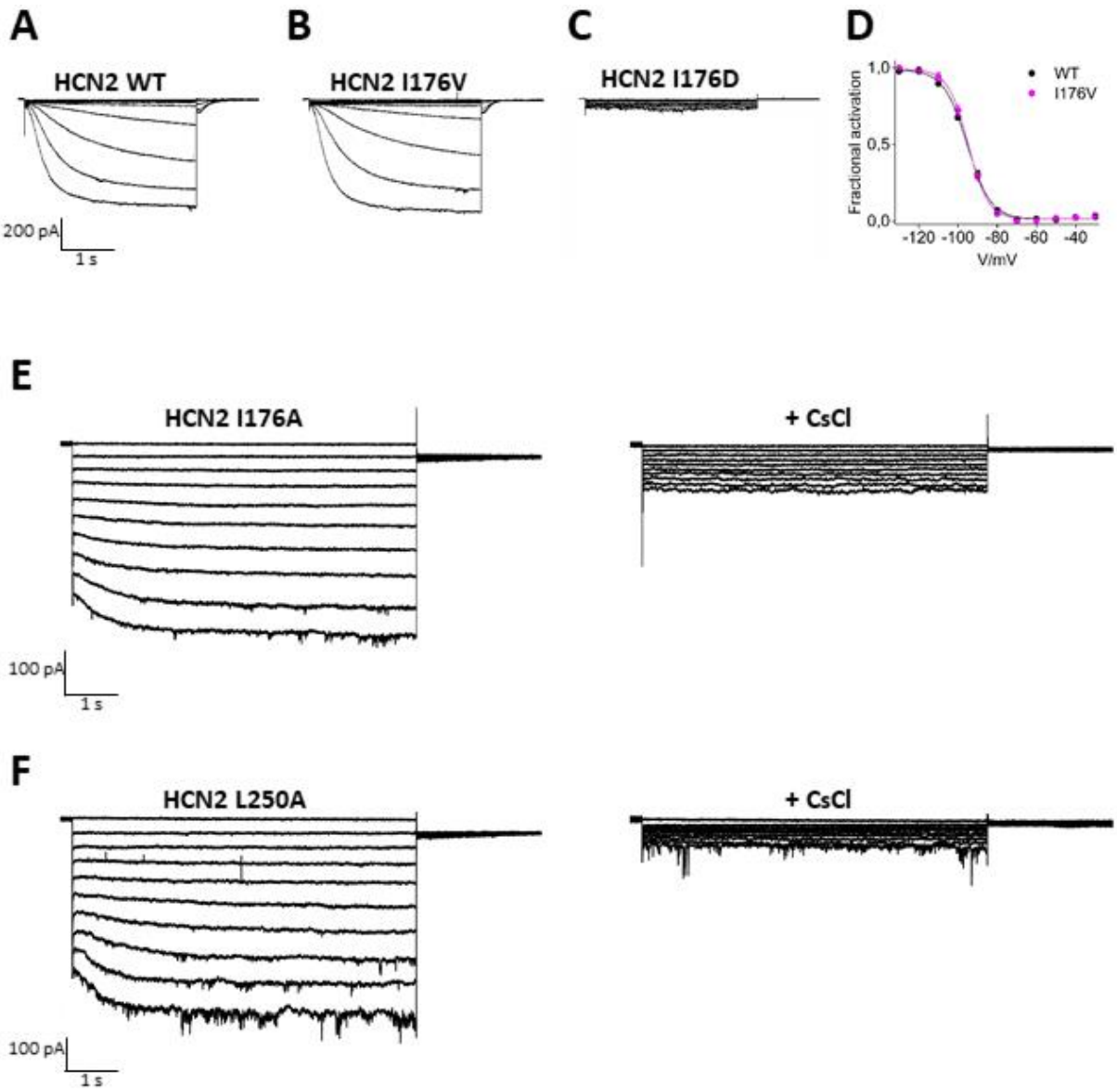

Figure 4.10: Patch-clamp recordings of mHCN2 I176 and L250 tested variants.
***A-C**, Representative whole-cell currents recorded from HEK293T cells transiently expressing wild-type, I176V or I176D mouse HCN2 channels. The protocol used for the recording is described in material and methods. **D**, Mean tail current activation curves of wild-type (black) and I176V (magenta) mutant channels. Lines show data fit to a Boltzmann function providing half activation potential (mean $V_{1/2}$ ± SEM) and inverse slope factor (mean k ± SEM) values as follow: $V_{1/2}$ = - 95,3 ± 0,5 mV, k = 6 ± 0,5 (wild-type); $V_{1/2}$ = -94,9 ± 0,4 mV, k = 5,1 ± 0,7 (I176V). $V_{1/2}$ values are not statistically different from wild-type mHCN2 (Student's T-test).*
***E,** Representative whole-cell current recorded from a cell expressing HCN2 I176A mutant channel before (left) and after 1 minute from the application of 2mM CsCl to the external solution (right). **F**, Representative whole-cell current recorded from a cell expressing HCN2 L250A mutant channel before (left) and after 1 minute from the application of 2mM CsCl to the external solution (right)*

We then reproduced the key experiments on hHCN1 channel in order to understand if the effects of the substitutions are conserved between the isoforms. As expected, when we placed a Valine residue in position 134 (that corresponds to 176 in HCN2), we recorded a current that was not distinguishable from the one generated by the wild-type channel (n=5) (Fig 4.11-B and -D). However, when we expressed the I134A mutant channel in HEK293T, none of the cells that we tested showed any HCN-like current, neither after 24h nor after 48h from the transfection (n=27) (Fig 4.11-C). These results indicate that the substitution of isoleucine residue in position 134 probably causes in HCN1 a much more substantial alteration of the trafficking than in HCN2, making it impossible to study the functional role of such hydrophobic residue in HCN1 isoform. At the same time, it suggests that in HCN1 too this residue plays a crucial role in either channel folding and/or functioning.

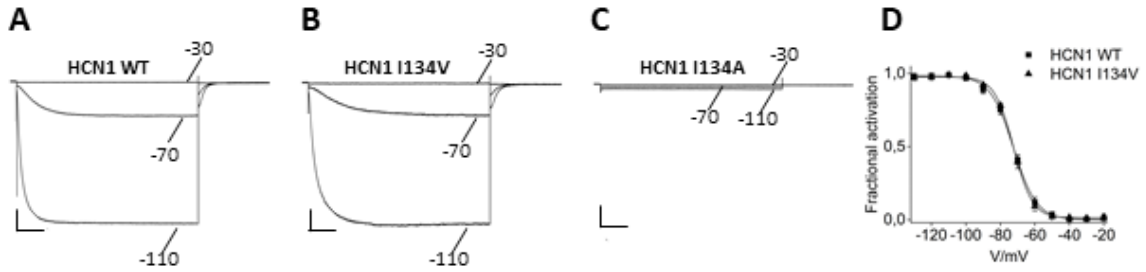

Figure 4.11: Patch-clamp recordings of hHCN1 I134 tested variants.
***A-C**, Representative whole-cell currents recorded, at the selected indicated voltages, from HEK293T cells transiently expressing wild-type, I134V or I134A human HCN1 channels. The protocol used for the recording is shown in material and methods. Scale bars represent 200pA and 1sec. **D**, Mean tail current activation curves of wild-type (black triangles) and I134V (black squares) mutant channels. Lines show data fit to a Boltzmann function providing half activation potential (mean $V_{1/2}$ ± SEM) and inverse slope factor (mean k ± SEM) values as follow: $V_{1/2}$ = - 72,4 ± 0,8 mV, k = 6,7 ± 0,3 (wild-type); $V_{1/2}$ = -72,4 ± 0,5 mV, k = 5,5 ± 0,4 (I134V). $V_{1/2}$ values are not statistically different from wild-type hHCN1 (Student's T-test)*

In conclusion, we identified an extended hydrophobic surface located between the base of TM S1 and S2 and S3 helixes and the underlying loop connecting the HCN domain to the first transmembrane segment (see Fig. 4.1). From both electrophysiological and the cellular localization experiments we concluded that I177 residue of HCN domain is crucial in controlling the proper traffiking of HCN channel to the plasma membrane (Fig. 4.7 and 4.8). Nevertheless, because of the position of I177, which interacts the TM S1-S2 (i.e. with the VSD), we cannot exclude that such

residue contributes to control the voltage dependent gating of HCN channels. In agreement with this theory, permissive mutations of the neighbouring residue I176 severely affect the voltage dependent gating (Fig 4.10).

Taken together, these data suggest that the HCN domain loop plays two crucial roles, tightly connected to each other: by maintaining the proper architecture of the VSD, it controls both the proper traffiking of the channel and the proper functioning of the VSD, i.e. allows proper communication between the VSD and the pore. Interestingly, in HCN1 the integrity of such hydrophobic pocket seems to be more critic for the trafficking compared to HCN2 (Fig. 4.10 and 4.11).

4.3 The second hydrophobic interaction sets the $V_{1/2}$ and is necessary for the cAMP response

In HCN1 channel, while the S4 segment is almost linear, the C-terminal portion of S1 helix bends, opening up a pocket between the two helixes (Fig 4.12). This cavity hosts the hydrophobic side chains of Y138 (from the HCN domain loop), I284 and M287 (both from the S4 helix) that create a hydrophobic pocket in which the side chain of aminoacid F109 (from the HCN domain HCNb helix) is inserted. This interaction brings the HCNb helix close to the membrane where it forms a sort of a plug for the cavity (Fig. 4.12).

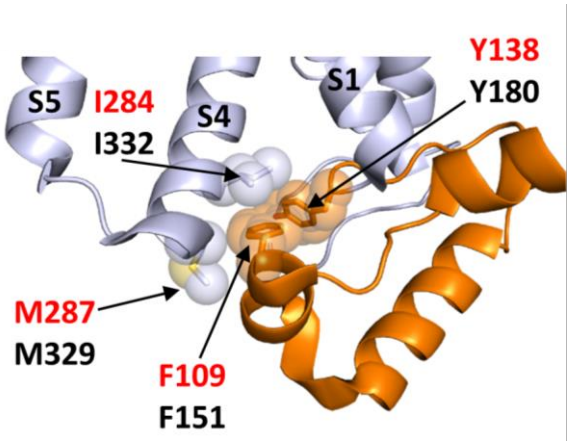

Figure 4.12: Detailed view of the "second hydrophobic pocket". The side chain of the amino acids involved in the hydrophobic interactions are shown as sticks depicted with the same colour of the sourcing main chain. Corresponding Van der Waals spheres have the same

colour code. Numbers referring to hHCN1 or mHCN2 aminoacid sequence are coloured in red or black respectively.

The F109 residue appears to be a key point for a putative contact between the HCN domain and the VSD. In order to test this hypothesis, we substituted F151A of mouse HCN2 channel (that corresponds to F109 in hHCN1) with a Glutamic acid residue with the aim to use the negative charge to prevent side chain insertion into the hydrophobic pocket. The HCN2 F151E mutant was expressed in HEK293T cells and whole-cell patch-clamp experiments were performed both in absence and in the presence of cAMP that was added to the pipette solution as described in material and methods. The results show that in the absence of cAMP the half activation voltage of the F151E mutant is shifted towards positive potentials of +34,7 ± 0,94 mV (n=3) compared to the wild-type (Fig. 4.13-B and Fig. 4.14). Addition of 15µM cAMP (a saturating concentration for HCN2) to the pipette solution caused, in the wild type channel, the expected facilitation of channel opening indicated by an increase in maximal current and a right shift (+15,7 ± 0,5 mV, n=8) in the channel activation curve (Fig. 4.13-A and Fig. 4.14). When the same concentration of cAMP was added to the F151E mutant both the current and the derived activation curve appeared indistinguishable from the wild-type (Fig. 4.13-B and Fig. 4.14). Moreover, we observed a strong decrease in the number of GFP positive (GFP+) cells that express a measurable HCN current (from 100% of the wild-type to about 10%; N=31) indicating that disruption of this hydrophobic interaction could affect the trafficking of the channel to the plasma membrane. We further analysed this interaction in order to test whether the effect of the F151 with E substitution was effectively due to the destabilization of the hydrophobic plug provided by the Phenylalanine residue and not to an alteration of the overall structure of the HCN domain.

To this end, we substituted the F151 residue with a set of hydrophobic residues (Ala, Val, Met, Trp) in order to gradually increase the length of their side chain. In this experiment we expected to observe a stepwise rescue of the wild-type properties. We started by introducing an Alanine which has the shortest side chain. When expressed in HEK293T cells, the F151A mutant showed a positive shift of the activation curve of +13 ± 0,4 mV (n=8), less than half of the shift measured with F151E (Fig. 4.13-C and Fig. 4.14). Moreover, the mutant channel responded to cAMP. When we added 15 µM of cAMP to the pipette solution, we measured a right

shift of +16,7± 0,9 mV (n=7) in $V_{1/2}$, not statistically different from that recorded with the wild-type channel (Fig 4.13-C and Fig 4.14). This suggests that the short hydrophobic side chain of Alanine is sufficient to rescue the effect of cAMP but is not able to completely re-establish the correct value of the $V_{1/2}$ in the resting channel. We further proceeded by inserting a Valine, a Methionine and a Tryptophan residue in this position. In the case of the F151V mutant we measured a small positive shift of the $V_{1/2}$ value of +4,4± 0,6 mV (n=9), while for the F151M and F151W mutants the shift was of +0,9 ± 0,9 mV (n=5) and +2,3± 0,7 mV (n=5) respectively (Fig. 4.13-D, -E and -F; Fig. 4.14). The administration of 15 µM cAMP to these three mutants caused a shift of the activation curve that was again comparable to those of the wild-type channel (Fig. 4.13-D, -E and -F; Fig. 4.14).

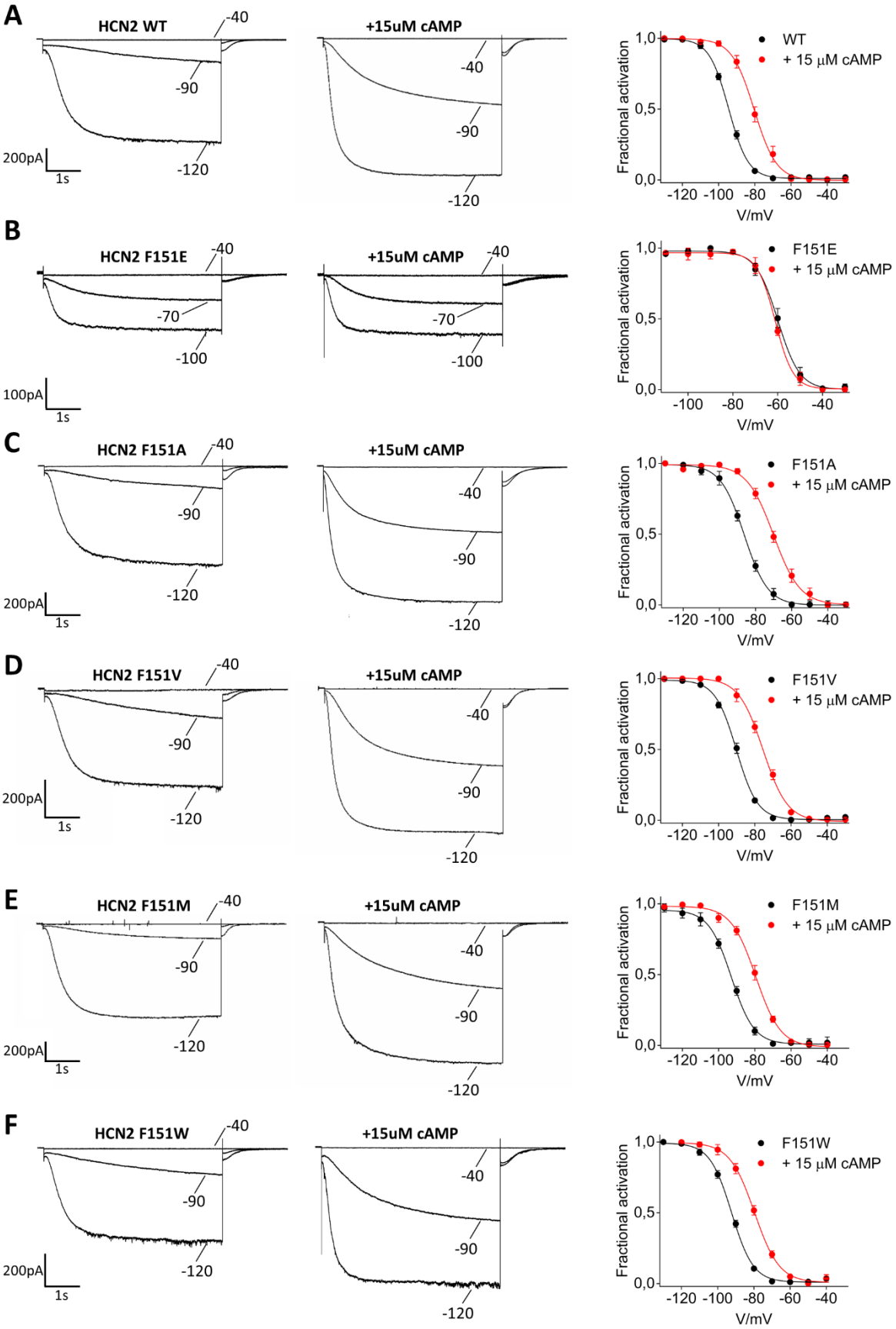

Figure 4.13: Patch-clamp recordings of mHCN2 F151 tested variants.

*Representative whole-cell currents recorded, at the selected voltages, from HEK293T cells transiently expressing wild-type (**A**), F151E (**B**), F151V (**C**), F151V (**D**), F151M (**E**) or F151W (**F**) mHCN2 channel both in the absence and in the presence of cAMP as indicated. The protocol used for the recording is described in material and methods. The right panels show mean tail current activation curves of the indicated mutant in the absence (black circles) and in the presence of cAMP (red circles). Lines show data fit to a Boltzmann function providing half activation potential and slope factors reported in Figure 4.14 legend.*

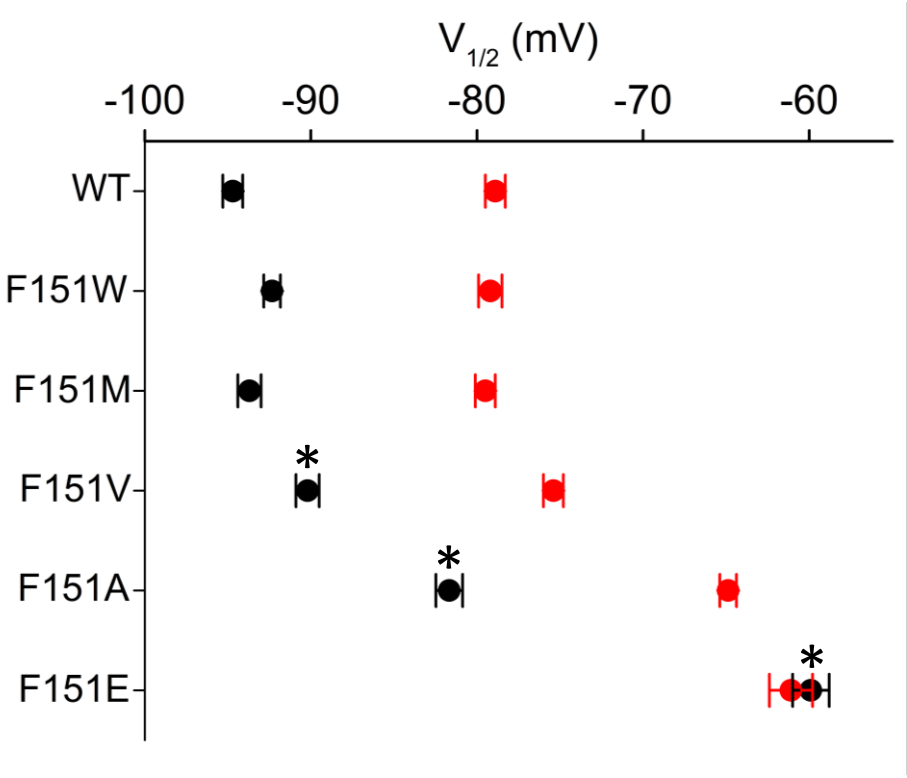

Figure 4.14: Mean half activation potential ($V_{1/2}$ ± SEM) values of the Phenylalanine 151 mutants in the absence (black circles) and in the presence of 15µM cAMP (red circles). Values derive from data showed in Figure 4.13. Mean half activation potentials ($V_{1/2}$ ± SEM) and inverse slope factor (mean k ± SEM) values obtained from the fitting of activation curves showed in Figure 4.8 are as follow: $V_{1/2}$ = -94,6 ± 0,5 mV, k = 6,3 ± 0,3 (wild-type); $V_{1/2}$ = -78,9 ± 0,6 mV§, k = 6,7 ± 0,5 (wild-type + 15µM cAMP); $V_{1/2}$ = -92,3 ± 0,5 mV, k = 6 ± 0,5 (F151W); $V_{1/2}$ = -79,2 ± 0,7 mV§, k = 6,8 ± 0,7 (F151W + 15µM cAMP); $V_{1/2}$ = -93,7 ± 0,7 mV, k = 6,2 ± 0,8 (F151M); $V_{1/2}$ = -79,5 ± 0,6 mV§, k = 6,8 ± 0,4 (F151M + 15µM cAMP); $V_{1/2}$ = -90,2 ± 0,7 mV, k = 5,8 ± 0,7 (F151V); $V_{1/2}$ = -75,5 ± 0,6 mV§, k = 6,7 ± 0,6 (F151V + 15µM cAMP); $V_{1/2}$ = -81,6 ± 0,8 mV*, k = 6,5 ± 0,4 (F151A); $V_{1/2}$ = -64,9 ± 0,5 mV§, k = 7,3 ± 0,8 (F151A + 15µM cAMP); $V_{1/2}$ = -59,9 ± 1,1 mV*, k = 4,9 ± 0,7 (F151E); $V_{1/2}$ = -60,1 ± 1,3 mV, k = 4,± 0,9 (F151E + 15µM cAMP). *p<0.05 by One-way ANOVA with Fisher's test compared to wild-type HCN2. §p<0.05 by Student's T-test compared to untreated condition.*

These results are consistent with the view that, substituting the F151 residue with a Glutamic acid, destabilizes the hydrophobic plug, or more precisely the interaction of F151 with the hydrophobic residues of S4. Therefore, with these data we provide a strong evidence that the HCN domain, via this hydrophobic interaction, plays two key

roles for the regulation of the channel: i) contributes to set the $V_{1/2}$ of the channel in the range of the physiological values; ii) is required for the cyclic nucleotide response.

In order to confirm that this interaction is not specific for HCN2 we reproduced the key experiments on hHCN1 channel. Thus, we mutated the F109 residue of hHCN1 (corresponding to F151 of HCN2 sequence) into both a Glutamic acid and an Alanine. The results are shown in Figure 4.15: none of the cells expressing hHCN1 F109E (n=22) mutant showed an HCN-like current, indicating that in HCN1 channel the integrity of this hydrophobic plug is probably more critical for the trafficking to the plasma membrane than in HCN2 (Fig 4.15-C). Instead, when we tested the F109A mutant, we observed a positive shift of the activation curve of about +7 ± 0,5 mV (n=5) mV (Fig 4.15-B and -D). These data are consistent with what we observed for HCN2 F151A mutant, suggesting that also in HCN1 channel the HCN domain plays a role in setting the $V_{1/2}$ in the range of physiologic values and possibly in mediating the cAMP response.

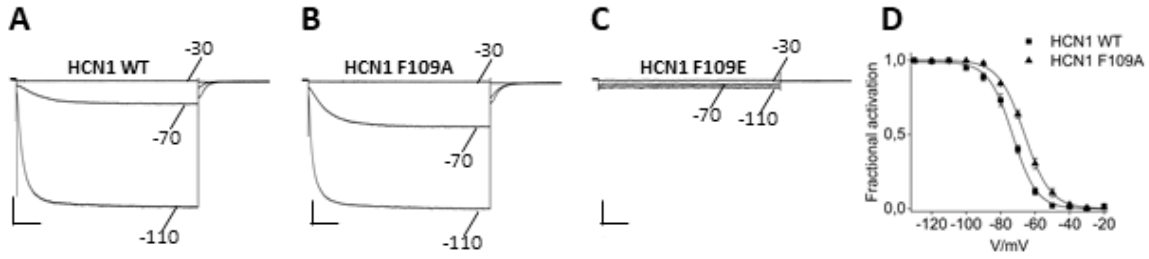

Figure 4.15: Patch-clamp recordings of hHCN1 F109 tested variants.
***A-C**, Representative whole-cell currents recorded, at the selected voltages, from HEK293T cells transiently expressing wild-type, F109A or F109E hHCN1 channels as indicated. **D**, mean activation curve of wild-type HCN1 (black circles) and F109A mutant (black triangles). Lines show data fit to a Boltzmann function providing half activation potential (mean $V_{1/2}$ ± SEM) and inverse slope factor (mean k ± SEM) values as follow: $V_{1/2}$ = -73 ± 0,4 mV, k = 7 ± 0,4 (HCN1 wild-type): $V_{1/2}$ = -66 ± 0,3mV*, k = 7,5 ± 0,3 (F109A). *p<0.05 by Student's T-test compared to wild-type hHCN1.*

In order to provide further details about this hydrophobic pocket, our collaborators in TU-Darmstadt (Technische Universität Darmstadt) have run a molecular dynamic simulation using the hHCN1-apo structure (PDB_ID: 5U6O [3]) with the aim to analyse the stability of the F109 residue side chain within the hydrophobic core. To this aim, the distances between F109 and Y137 or F109 and I284 side chains (Fig. 4.12) during the whole 100ns of simulation were measured. The results are shown in

Figure 4.16: the distances between the side chains of the abovementioned residues were constant during the whole simulation, indicating that the side chain of F109 residue is always inserted in the hydrophobic pocket. Indeed, these results support the hypothesis of a strong and stable hydrophobic interaction between the HCN domain and VSD.

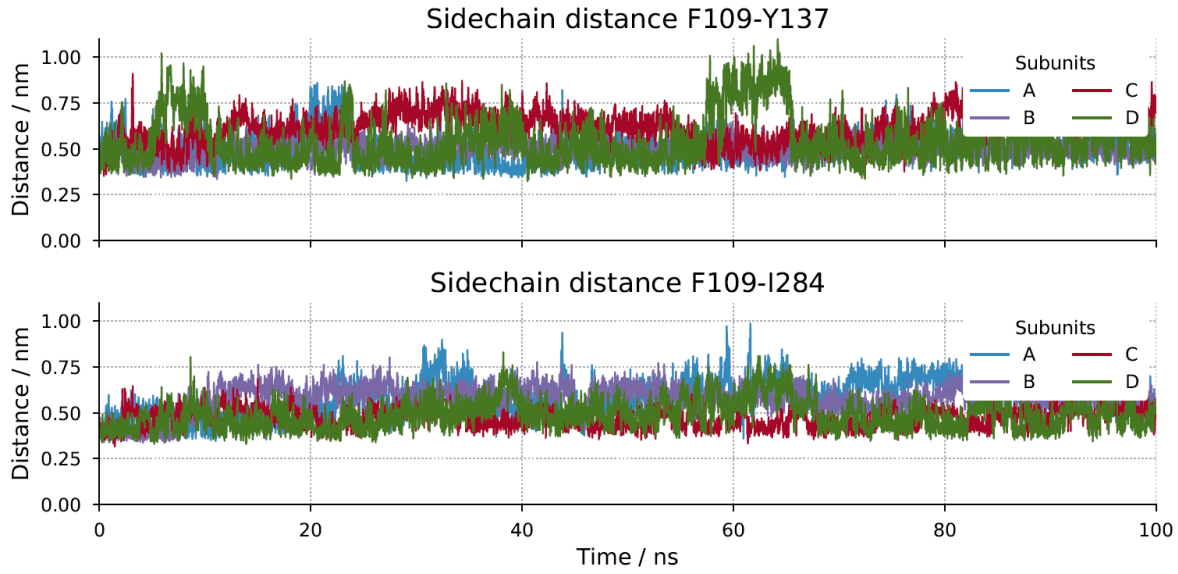

Figure 4.16: MD simulation on hHCN1 apo-structure (PDB_ID: 5U6O).
Time dependent distances between F109 and I283 or Y138 as running average over 1 ns are represented in top or bottom panel respectively. Distances between F109 and I284 or Y138 were calculated using representative atoms on the side chains: CZ for F109, CG1 for I284, and CZ for Y138. Different colours represent the distances calculated for each subunit.

4.4 Interactions with the C-linker are necessary for the response to the cyclic nucleotide

Immediately below the pore of HCN1, the A' and B' helices of the C-linker of the four subunits assemble into a flat, disc-like structure, which is surrounded by the four HCN domains (Fig 4.17-A). Each HCN domain is connected, by means of electrostatic interaction, to the A' helix of one monomer from one side and to the B' helix of the neighbour monomer from the other side. Indeed, R112 residue on HCNb helix of HCN domain forms a salt-bridge with residue E436 of B' helix of the C-linker from the adjacent subunit; residue K422 on the B' helix of the C-linker from the

opposite subunit interacts with the carbonyl group of the main chain of the residue M113 of the HCN domain (Fig 4.17-A and -B). Therefore, we speculated that, via these contacts, the conformational changes that occur in the C-linker upon cAMP binding to the CNBD are transmitted to the HCN domain and finally to the VSD allowing the facilitation of the channel opening. Based on this working hypothesis, mutations that neutralize these charged residues, most probably when combined together, should severely affect cAMP signaling of HCN channels.

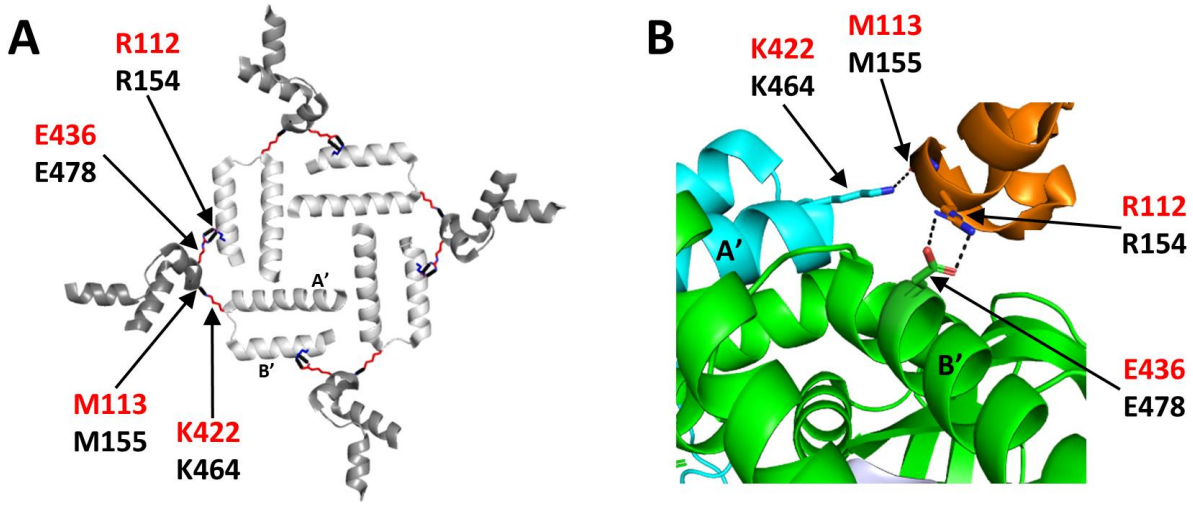

Figure 4.17: Electrostatic interactions connect the HCN domain with the C-linker.
A, *Top view of the structure showing the disc of the four C-linker (light grey) surrounded by the four HCN domains (dark grey). It is well visible how a single HCN domain contact two consecutive C-linkers by mean of the two salt-bridges. In red and in blue are respectively represented the positively and negatively charged side chains of the residues engaging electrostatic interactions.* ***B,*** *detailed view of the salt-bridge interactions that the HCN domain (orange) establishes with the C-linker of both the adjacent (green) and opposite subunit (light blue). The side chains of the residues engaging the electrostatic interactions are shown as sticks. Numbers referring to hHCN1 or mHCN2 aminoacid sequence are coloured in red or black respectively.*

It is worth noting that, carefully looking at the contacts that R112 residue displays in the cryo-EM HCN1 structure, we found that R112 might develop an electrostatic interaction with the carbonyl group of the main chain of T288 residue of TM S4, (Fig. 4.18). On the basis of this finding, we speculate that R112 plays a double role: i) by contacting E478 of B' helix of C-linker, it connects HCN domain with the C-linker and thus links the VSD-HCN domain functional unit to the cytosolic region of the channel; ii) it contributes to anchor the HCN domain to the overheading VSD, thus helping in the maintenance of the correct position of the “second hydrophobic pocket”. In this

view, neutralizing the positive charge of R112 residue (e.g. introducing R112A mutation), should cause not only the disconnection of the C-linker (by breaking R112-E436 salt bridge), but also the destabilization of the "second hydrophobic pocket" integrity. Since at this stage we were focused on clarifying the role of the interaction between HCN domain and the C-terminus of the protein, we decided to mutate E436 residue without touching its partner (R112) in order to selectively disrupt the interaction between the C-linker and the HCN domain, without perturbing the stability of "second hydrophobic pocket".

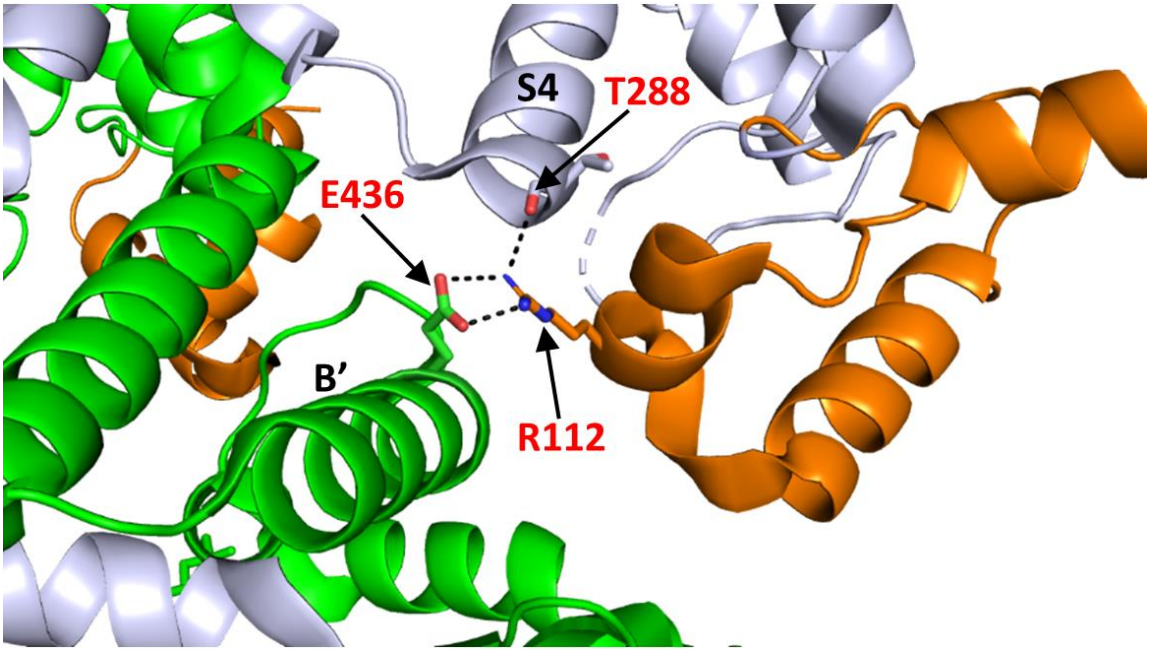

Figure 4.18: Detailed view of the salt-bridge interactions established by R112 residue (HCN domain, orange) with both E436 residue (C-linker belonging to the adjacent subunit, green) and T288 main chain CO^- group (TM S4, grey). Numbers refers to hHCN1 sequence.

Therefore, we exchanged the two charged residues, E478 and K464 in HCN2, with an Alanine; the two substitution were introduced both individually (K464A and E478A single mutants) and in combination (K464A-E478A double mutant). Patch-clamp experiments on HEK293T cells expressing the mutants were performed both in the presence and in the absence of cAMP. Analysing K464A mutant currents, we observed a right shift in the $V_{1/2}$ of +9,2 ± 1,3 mV (n=10) towards positive potentials compared to the wild-type (Fig.4.19-B). When we added 15 µM of cAMP to the pipette solution, we measured a right shift of +15,7 ± 0,94 mV (n =7) in the $V_{1/2}$ and

the expected increase of the maximal current, not statistically different from that recorded in the wild-type (Fig.4.19-B). Instead, when we expressed the E478A mutant in the absence of the cyclic nucleotide we observed a left shift in the $V_{1/2}$ of -18,6 ± 1,39 mV (n=7) (Fig.4.19-C); the addition of 15 µM of cAMP still caused a wt-like right shift in the $V_{1/2}$ of +13,5 ± 0,95 mV (n=6) accompanied by the increasing effect of the maximal current (Fig.4.17-C).

We therefore proceeded testing the double K464A-E478A mutant: in the absence of cAMP the $V_{1/2}$ value was not statistically different from the one of the wild-type (-3,9 ± 1,5 mV, n=8) already indicating that the two single effects of the mutation on $V_{1/2}$ are additive; moreover, when we added 15µM of cAMP in the pipette solution, we could not measure any ligand-induced effect, neither a shift of the activation curve nor the increase in the maximal current (Fig.4.19-D). To explore the possibility that the lack of effect was due to a decrease in cAMP affinity of the channel, we increased the cAMP concentration to 100µM: also in this case we observed no effect of the ligand, as shown by the activation curve plotted in Fig 4.19-D (n=4), finally confirming that the double mutant does not respond to cAMP.

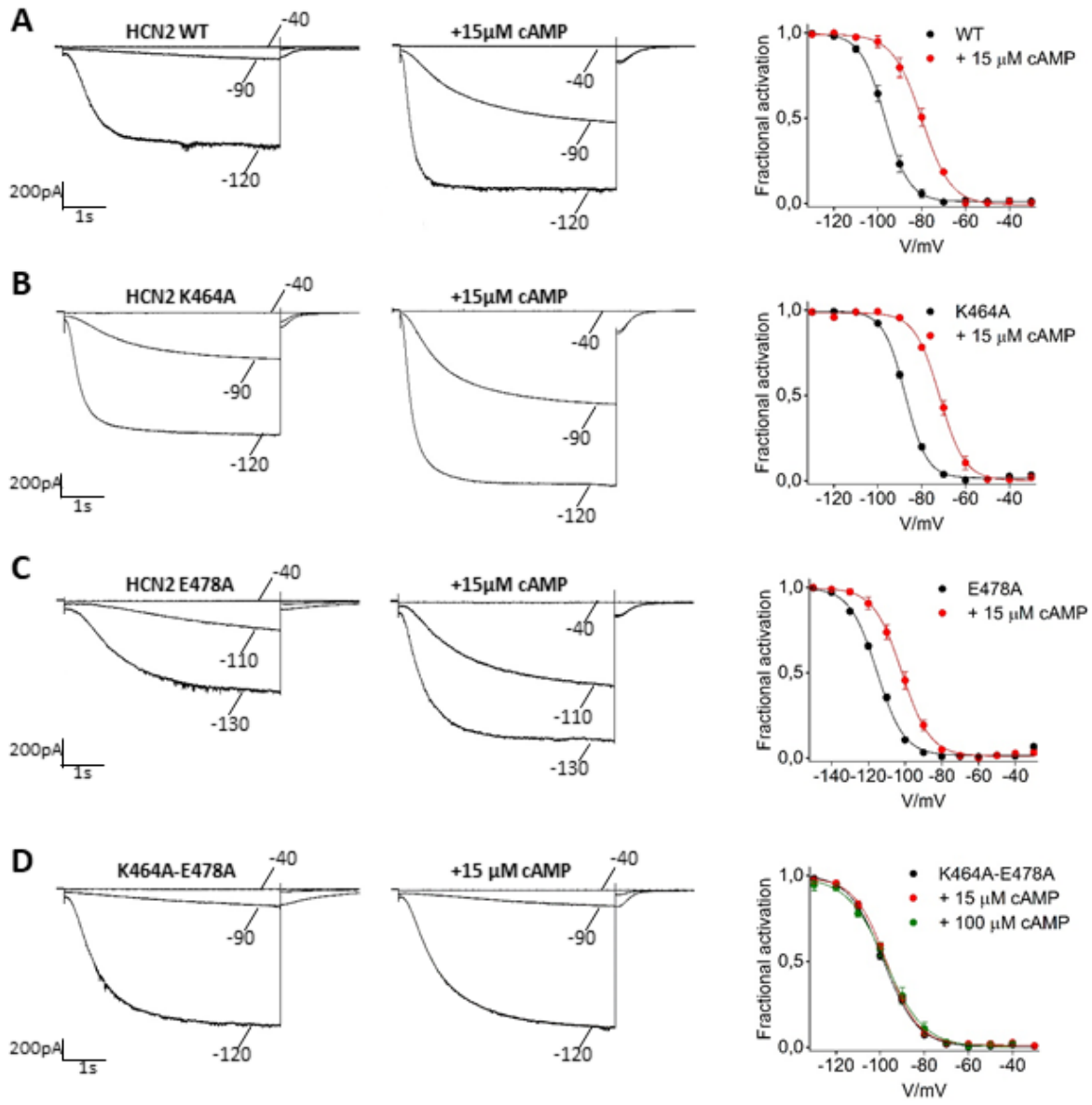

Figure 4.19: Patch-clamp recordings of mHCN2 K464 and E478 tested variants.
*Representative whole-cell currents recorded, at the selected voltages, from HEK293T cells transiently expressing wild-type (**A**), K464A (**B**), E478A (**C**), K464A-E478A (**D**), both in the absence and in the presence of cAMP as indicated. The protocol used for the recording is described in material and methods. The right panels show mean tail current activation curves of the indicated mutant in the absence (black circles) and in the presence of 15 µM or 100 µM of cAMP (red and green circles respectively). Lines show data fit to a Boltzmann function providing half activation potential (mean $V_{1/2}$ ± SEM) and inverse slope factor (mean k ± SEM) values as follow: $V_{1/2}$ = - 96,7 ± 1,2 mV, k = 6,3 ± 0,5 (wild-type); $V_{1/2}$ = - 80,2 ± 1,5mV§, k = 6,8 ± 0,7 (wt + 15µM cAMP mutant); $V_{1/2}$ = -87,5 ± 0,5 mV*, k = 5 ± 0,4 (K464A mutant); $V_{1/2}$ = -71,8 ± 0,8 mV§, k = 5,6 ± 0,3 (K464A mutant + 15µM cAMP); $V_{1/2}$ = -115,3 ± 0,7 mV*, k = 7,4 ± 0,5 (E478A mutant); $V_{1/2}$ = -101,8 ± 0,5 mV§, k = 7,7 ± 0,4 (E478A mutant + 15µM cAMP); $V_{1/2}$ = -100,6 ± 0,95 mV, k = 5,9 ± 0,4 (K464A-E478A mutant); $V_{1/2}$ = -97,3 ± 0,4 mV, k = 6,9 ± 0,5 (K464A-E478A mutant + 15 µM cAMP). $V_{1/2}$ = -97,4 ± 1,35 mV, k = 8 ± 0,9 (K464A-E478A + 100 µM cAMP). *p<0.05 by One-way ANOVA with Fisher's test compared to wild-type HCN2. §p<0.05 by Student's T-test compared to untreated condition.*

The $V_{1/2}$ analysis of the single mutant channels showed that, individually abolishing the two interactions, led in one case to an increase of the probability of channel opening (K464A mutant), while, in the other, caused the opposite effect (E478A mutant). This suggests that HCN domain exerts two different effects on the C-linker.

By mean of the connection with the B' helix of the C-linker (Fig.4.17-A), the HCN domain might act as an actuator element of the VSD, in the sense that VSD uses HCN domain to facilitate the rotation of the C-linker elbow during the opening of the pore. In agreement with this working hypothesis, the removal of the E478 (elbow) - R112 (HCN domain) interaction should cause the requirement of an additional energy to gate the channel (i.e. to rotate the C-linker), because the actuator element of the VSD, the HCN domain, is no longer connected to the C-linker elbow. This additional energy needed to move the C-linker can be visualized as a hyperpolarizing shift of the voltage dependent opening of the mutant channel. Indeed, this is exactly what we saw when we measured the E478A mutant (Fig. 4.19-C). As a consequence of this, we speculate that, when HCN domain C-linker elbow connection is lost, the only way for the VSD to rotate the C-linker is to act on the overheading TM S5-S6 pore helices, which are physically attached to the C-linker.

On the other side, the connection between the HCN domain and the C-linker A' helix (Fig 4.17-A) might have a role in maintaining the C-linker elbow in a given conformation. The break of this interaction (K464A mutant) probably causes a slight movement of the elbow and this movement affects the voltage dependent gating of the channel. Since the $V_{1/2}$ of the K464A is shifted towards more depolarized voltages, i.e. the energy required by the VSD to gate the pore is smaller (Fig. 4.19-B), we can speculate that the removal of such connection with the HCN domain, causes a slight movement of the C-linker elbow in the typical direction that causes the opening of the pore.

Finally, the most interesting aspect of this result is that, disrupting both the two salt-bridges that connect the C-linker to the HCN domain, the channel become insensitive to the cAMP modulation, i.e., the cAMP-induced movement of the C-linker are not affecting anymore the VSD. This functionally proves the above stated working hypothesis: these C-linker residues play a crucial role in the mechanical transmission of cAMP signalling form the cytosolic region of the channel to the transmembrane VSD via the HCN domain. This behaviour, in our view, clearly indicates that the HCN

domain mechanically connects the movement of the C-linker to the VSD. If we add these new achievements with the evidence that the Phenylalanine of the second hydrophobic pocket is necessary for the cAMP response, we can suggest a new model that could explain how the binding of the cAMP is converted in the facilitation of the channel opening: the cyclic nucleotide binds to the CNBD inducing the movements in the overlying “shoulder” of the C-linker. The shoulder generates a rotational movement of “elbow” element, i.e. A’ and B’ helices, that is transmitted to the HCN domain and via the two hydrophobic pockets to the VSD resulting in the shift in $V_{1/2}$. We find particularly meaningful the interaction with S4 driven by the Phenylalanine of the second hydrophobic pocket. Indeed, mutating this residue too, results in the loss of response to cAMP. Nonetheless, our results show that also the first hydrophobic pocket and in particular the two Isoleucine residues on HCN domain loop are involved in controlling the VSD and might be involved in cAMP response as well.

To test whether this proposed mechanism is common to all HCN isoforms, we introduced the double K422A-E436A mutation in hHCN1 (corresponding to K464A-E478A of mHCN2). It is worth noting thatHCN1 does not apparently respond to the application of exogenous cAMP (Fig 4.20-A) because this HCN isoform has an extremely high affinity for the ligand and thus it is already saturated by endogenous cAMP [54]. Because of this, we have compared the effect of the double mutation to the wild-type channel without applying cAMP in the patch pipette, and also to the cAMP-insensitive mutant R549E [55]. Indeed, this mutation reduces cAMP affinity of the CNBD by 100X and results in a negative shift of $V_{1/2}$ confirming that HCN1 is fully saturated by endogenous cAMP. The $V_{1/2}$ of the hHCN1 K422A-E436A double mutant was left shifted of -7,5 ± 0,45 mV (n=11) compared to the wild-type. Strikingly, approximately the same shift (-8,7 ± 0,65 mV, n=5) was obtained by introducing on the wild-type channel, the mutation R549E that prevents cAMP binding to the CNBD (Fig. 4.20-B). Since the double mutation K422A-E436A, or the cAMP-insensitive R549E mutation gave not statistically different results we concluded that, as in HCN2, breaking the interactions of HCN domain with the C-linker, removes the response to cAMP of the channel. To definitively confirm this result, we performed two parallel experiments: i) we measured the double mutant by adding 100µM of cAMP to the

pipette solution; ii) we introduced the cAMP-insensitive R549E mutation in the double mutant. As expected, both the activation curves of K422A-E436A in the presence of 100 µM cAMP (n=4) and the one of the triple K422A-E436A-R549E overlapped (n=10) (Fig 4.20-C). these results let us to conclude that the previously proposed mechanism of action of cAMP seems to be a common mechanism of HCN channels.

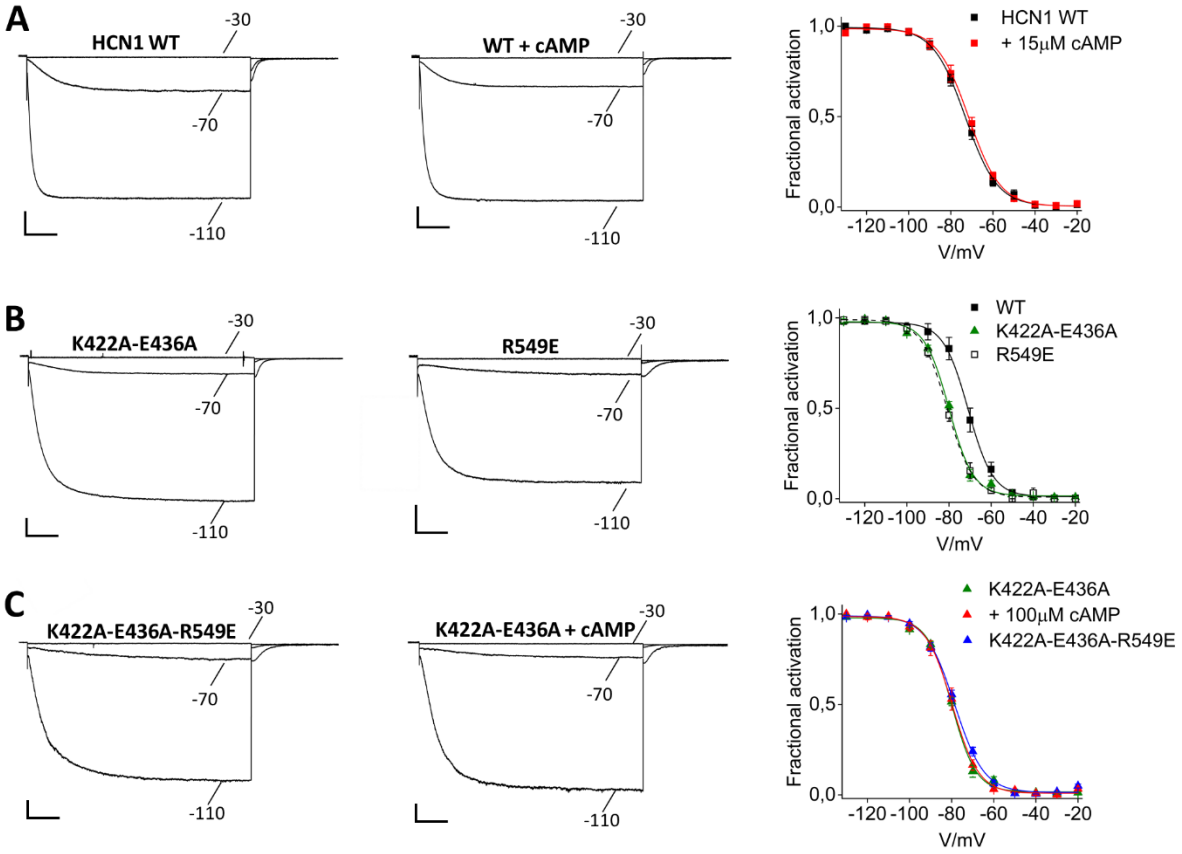

*Figure 4.20: Patch-clamp recordings of hHCN1 K422A-E436A double mutant. Representative whole-cell currents recorded, at the selected voltages, from HEK293T cells transiently expressing wild-type (**A**), K422A-E436A (**B**), R549E (**B**), K422A-E436A-R549E (**C**) hHCN1 channels in the absence and in the presence of cAMP where indicated. The protocol used for the recording is described in material and methods. The right panels show mean tail current activation curves of the indicated mutant in the absence (black circles) and in the presence of 15 µM or 100 µM of cAMP (red and green circles respectively). Lines show data fit to a Boltzmann function providing half activation potential (mean $V_{1/2}$ ± SEM) and inverse slope factor (mean k ± SEM) values as follow: $V_{1/2}$ = - 72,2 ± 0,4 mV, k = 7,7 ± 0,3 (HCN1 wild-type); $V_{1/2}$ = - 71,4 ± 0,9 mV, k = 7,4 ± 0,5 (HCN1 wild-type + 15µM cAMP); $V_{1/2}$ = -79,7 ± 0,2 mV*, k = 8 ± 0,2 (K422A -E436A); $V_{1/2}$ = -78,6 ± 0,4 mV, k = 6,9 ± 0,4 (K422A-E436A-R549E); $V_{1/2}$ = -79,7 ± 0,4mV, k = 6,2 ± 0,4 (K422-E436A + 100µM cAMP); $V_{1/2}$ = -80,9 ± 0,3 mV*, k = 6,2 ± 0,2 (R549E). *p<0.05 One-way ANOVA with Fisher's test compared to wild-type HCN1.*

.

4.5 HCN domain interactions with CNBD

The HCN1 structure provides little information about putative interactions of the HCN domain with the CNBD because in both, apo and holo structures, most of the side chains of CNBD are not assigned. Among the few that were assigned, Lysine 118 on the HCN domain points towards Aspartic acid 534 of the CNBD (Fig. 4.21). We therefore mutated the corresponding residue on HCN2, K160, into an Alanine in order to abolish any potential electrostatic interaction. When expressed in HEK cells, the K160A mutant showed a small positive shift of the $V_{1/2}$ of + 4,6 ± 0,4 mV (n=10) compared to the wild-type (Fig. 4.22-B and -D). The response to a saturating concentration of cAMP of this mutant appeared normal, as the addition of 15µM of cAMP caused the increase of the maximal tail current and a right shift in the $V_{1/2}$ of +14,1 ± 0,4 mV (n=6), not different from the wild-type (Fig. 4.22-B and -D). At lower concentration, 1µM, the mutant channel shifted by +9,7 ± 0,4 mV (n=10), about 2 times more than the wild-type (+4,4 ± 0,3 mV (n=8) (Fig. 4.22-B and -D). This indicated a higher affinity or efficacy for cAMP of the K160 mutant. We further substituted K160 with a glutamate in order to introduce an electrostatic repulsion with the putative partner on the CNBD (if any). In the absence of cAMP, the K160E mutant displayed a right shift in the $V_{1/2}$ of +10 ± 0,3 mV (n=10) compared to the wild-type, thus supporting the hypothesis that K160 could be interacting with a negatively-charged amino-acid on the CNBD (Fig. 4.22-C and -D). We then tested 15µM and 1µM cAMP concentrations: also in this case, saturating concentration (15µM) of the cyclic nucleotide caused a shift of $V_{1/2}$ of +14,8 ± 0,7 mV (n=5) similar to the wild-type, while 1µM of cAMP induced a shift of + 9,9 ± 0,5 mV (n=5) indicating that this mutant too has higher affinity than the wild-type to cAMP (Fig. 4.22-C and -D).

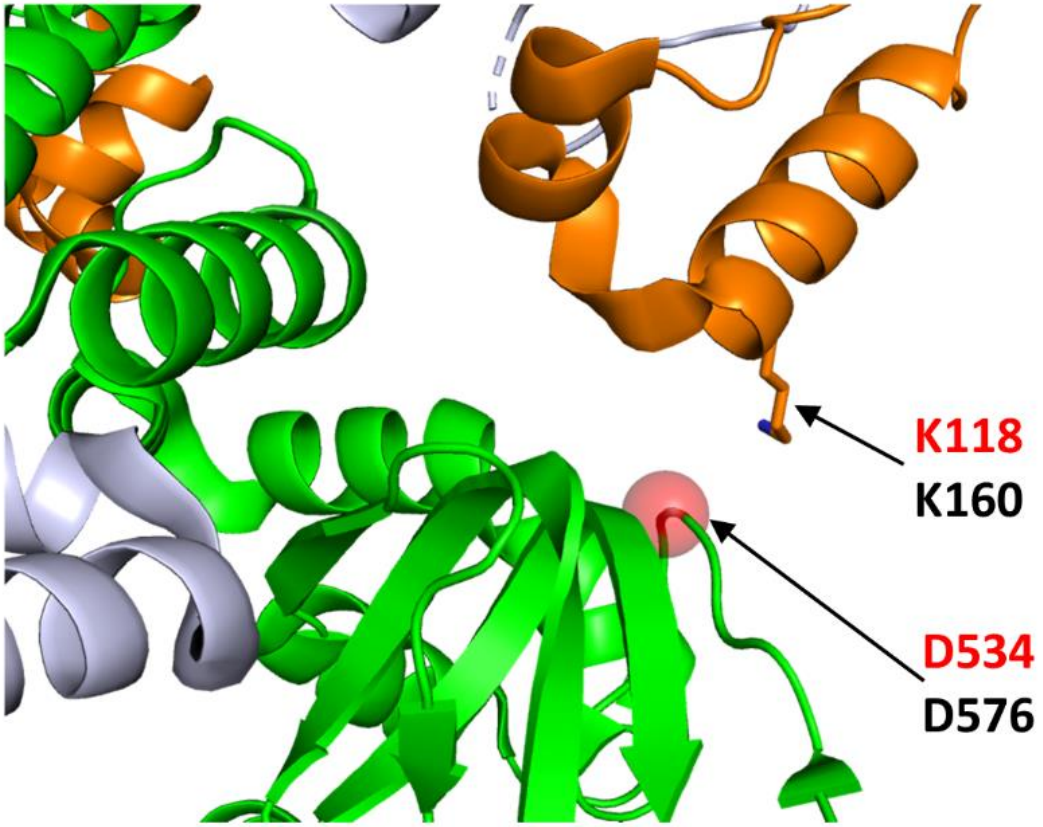

Figure 4.21: Putative electrostatic interaction between HCN domain and CNBD.
Two adjacent subunits of hHCN1 tetramer are coloured in grey or in green. HCN domain is shown in orange. Side chain of K118 residue of the HCN domain is represented as stick. Red sphere represents the position of the D534 residue on CNBD speculated to be the possible partner of an electrostatic interaction with the K118. Numbers referring to hHCN1 or mHCN2 aminoacid sequence are coloured in red or black respectively.

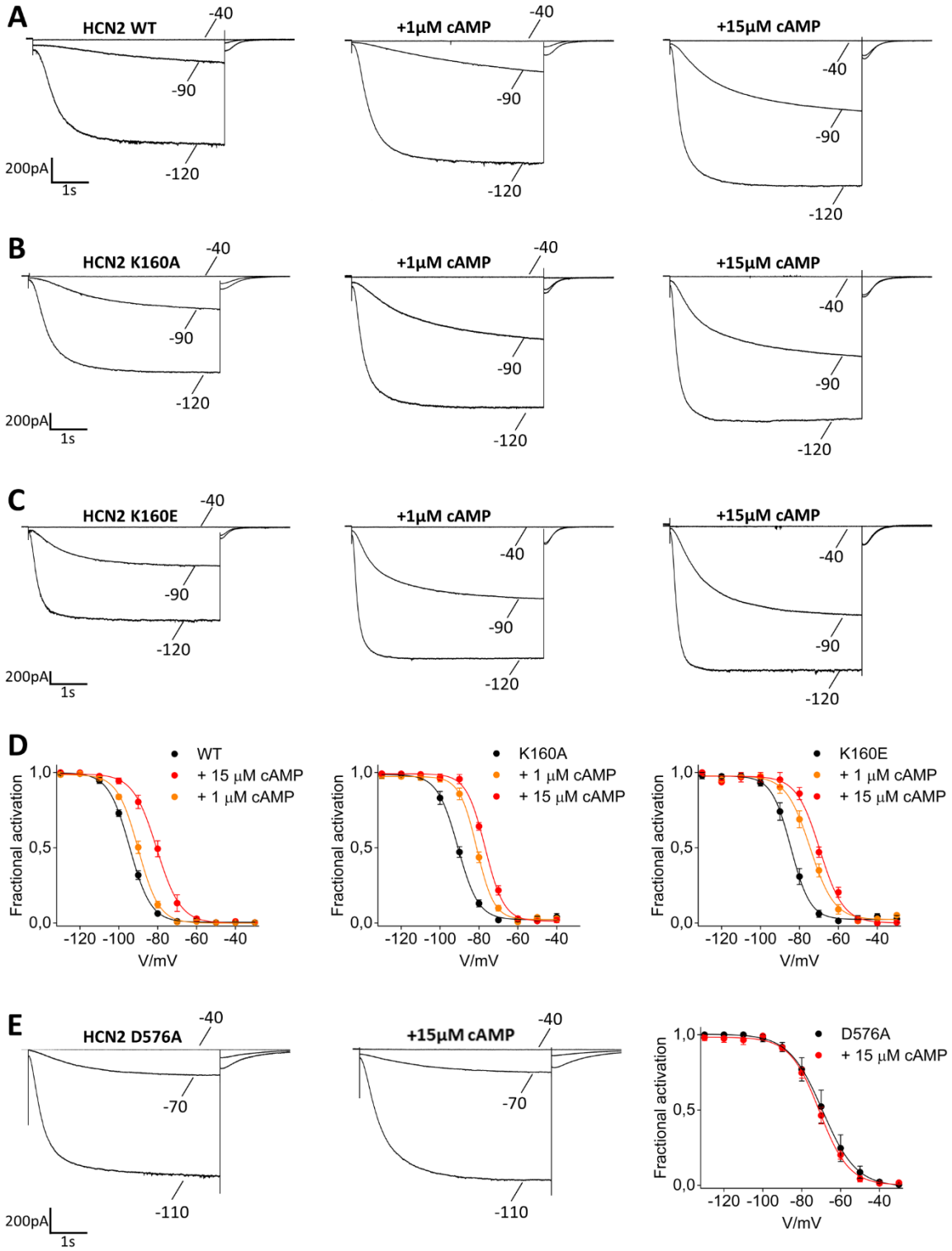

Figure 4.22: Patch-clamp recordings of mHCN2 K160 and D576 tested variants.
***A-C**, Representative whole-cell currents recorded, at the selected voltages, from HEK293T cells transiently expressing wild-type, K160A or K160E mHCN2 channels both in the absence and in the presence of 1µM and 15µM cAMP as indicated.*
***D**, Mean activation curves of WT (black, left) K160A (black, centre) and K160E (black, right) channels both the absence and in the presence of 1µM (orange) or 15µM (red) cAMP. Lines show data fit to a Boltzmann function provding half activation potential (mean $V_{1/2}$ ± SEM) and inverse slope factor (mean k ± SEM) values as follow: $V_{1/2}$ = -94,4 ± 0,6 mV, k = 5,5 ±*

0,5 (wild-type); $V_{1/2}$ = -90 ± 0,4 mV§, k = 5,4 ± 0,7 (wild-type + 1µM cAMP); $V_{1/2}$ = -80,5 ± 0,5mV§, k = 6,1 ± 0,4 (wild-type + 15µM cAMP); $V_{1/2}$ = -89,8 ± 0,7 mV, k = 5,3 ± 0,6 (K160A); $V_{1/2}$ = -80,8 ± 0,7mV§, k = 4,5 ± 0,8 (K160A + 1µM cAMP); $V_{1/2}$ = -76,8 ± 0,8 mV§, k = 4,9 ± 0,7 (HCN2 K160A + 15µM cAMP); $V_{1/2}$ = -84,4 ± 0,5 mV*, k = 5 ± 0,4 (HCN2 K160E); $V_{1/2}$ = -74,5 ± 0,6 mV§, k = 6,2 ± 0,4 (K160E + 1µM cAMP); $V_{1/2}$ = -69,6 ± 0,7mV§, k = 6 ± 0,6 (K160E + 15uM cAMP). **E**, Representative whole-cell currents recorded, at the selected voltages, from HEK293T cells transiently expressing mHCN2 D576A mutant channel both in the presence and in the absence of cAMP. Right panel displays activation curves D576A mutant channel both the absence (black) and in the presence of 15µM (red). Lines show data fit to a Boltzmann function provding half activation potential (mean $V_{1/2}$ ± SEM) and inverse slope factor (mean k ± SEM) values as follow: $V_{1/2}$ = -69,3 ± 1,2 mV*, k = 8,7 ± 0,4 (D576A); $V_{1/2}$ = -70,9 ± 0,6 mV, k = 7,5 ± 0,4 (D576A + 15µM cAMP). *p<0.05 by One-way ANOVA with Fisher's test compared to wild-type HCN2. §p<0.05 by Student's T-test compared untreated condition.*

To further better characterize the increase in the cAMP sensitivity, we measured the dose–response relationships of the $V_{1/2}$ shift against cAMP concentration in both the wild-type and K160E mutant. Fitting the Hill equation to data showed that indeed the mutant channel has a 4 times higher cAMP sensitivity compared to the wild-type (Fig 4.23).

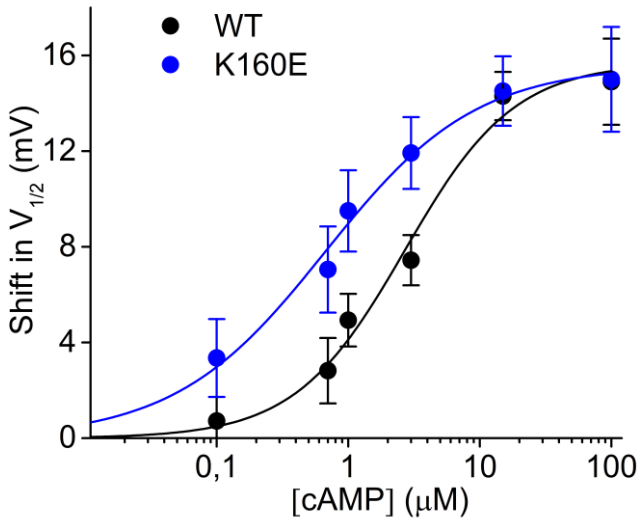

Figure 4.23: Whole-cell dose–response relationships of cAMP dependence of activation curve shift in cells expressing wild-type (black line) or K160E (blue line) mutant mHCN2 channels. Each datapoint is the average of 3–5 exposures. Parameters of Hill fitting of these curves are as follow (Kd ± SEM): Kd = 2,7 ± 0,6 µM (wild-type); Kd = 0,66 ± 0,11 µM (K160E).

Finally, we substituted the negatively charged D576 residue on the CNBD of mHCN2 with an Alanine in order to explore the possibility that this residue establishes the

electrostatic interaction with K160 residue of HCN domain. Analysis of mHCN2 D576A mutant showed a positive shift of +25,1 ± 0,3 mV (n=4) in the $V_{1/2}$. Moreover, addition of 15µM cAMP to the pipette solution did not further shift the $V_{1/2}$ (Fig 4.22-E). These results totally disagree with those obtained with K160A and K160E mutant, indicating that (at least in HCN2 channel) these residues do not form a salt bridge.

Moreover, when we substituted K108 in HCN1 (corresponding to K160 in HCN2) with the Glutamic acid, the activation curve of the mutant was indistinguishable from the one of the wild-type (Fig. 4.24), indicating that probably, this residue, is not involved in salt bridge interactions.

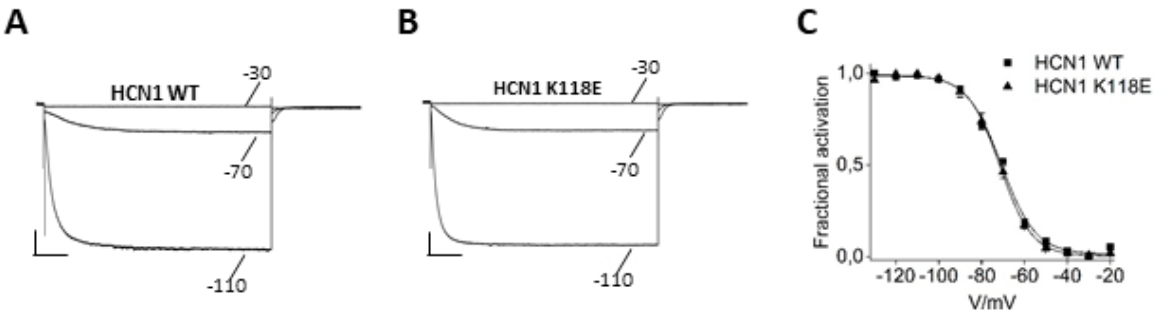

Figure 4.24: Patch-clamp recordings of hHCN1 K118E mutant.
***A-B**, Representative whole-cell currents recorded, at the selected indicated voltages, from HEK293T cells transiently expressing wild-type or K118E mutant hHCN1 channels. **C**, mean activation curve of wild-type HCN1 (black squares) and K118E mutant (black triangles). Lines show data fit to a Boltzmann function provding half activation potential (mean $V_{1/2}$ ± SEM) and inverse slope factor (mean k ± SEM) values as follow: $V_{1/2}$ = -70,8 ± 0,8 mV, k = 8 ± 0,7 (HCN1 wild-type): $V_{1/2}$ = -71,5 ± 0,4mV, k = 7,5 ± 0,3 (K118E mutant). Values are not statistically different from hHCN1 wild-type (Student's t-test).*

The different results that we found in HCN1 and HCN2 provide the indication that, in this point, HCN1 and HCN2 could be slightly divergent. Assuming that the K160 residue in HCN2 is interacting somewhere in the CNBD, the same aminoacid in HCN1(K118) does not do the same. This would be partially supported by the fact that in HCN1 structure the putative electrostatic interaction is not visible; indeed, in the presence of a stable and functional interaction, the side chain of a partner of K118 residue would be visible in the 3D density map of the structure. Moreover, the discordant results obtained with K160 and D576 mutants, indicates that in the structure of HCN2, the relative position of the HCN domain and the CNBD would be different from that reported for HCN1. This difference may also be strictly related to

the different cAMP sensitivity of the two isoforms, much higher in HCN1 than in HCN2 ($K_{1/2}$ = 0.06 µM (HCN1); $K_{1/2}$ = 0.10 µM (HCN2) [56]); indeed, the role of this potential interaction in HCN2 channel would be to keep the CNBD in a sort of low affinity conformation. If abolished, the channel is more sensitive to the cAMP (Fig. 4.23), becoming more similar to an HCN1.

4.6 HCN domain as a tool to modulate HCN channels gating

The finding that HCN domain can control the response of the channel to cAMP, inspired the following experiment in which a synthetic HCN domain peptide was used to interfere with the normal function of the native domain.

To this aim, we ordered a commercially synthetized peptide comprising the three helixes of the HCN domain (from aa 94 to 131 of hHCN1 sequence). The peptide was dissolved in the pipette solution and the cells, expressing HCN2 channels, were patched in whole-cell configuration in order to deliver the peptide to the cytosolic side of the channels.

Addition of 50µM of the synthetic HCN domain (hereafter sHD) to the pipette solution caused the right shift in the $V_{1/2}$ of +14 ± 0,5 mV (n=10), indicating that the isolated peptide is active and able to modulate the gating proprieties of the channel (Fig 4.25-B and -D). Increasing the concentration up to 100µM did not further shift the $V_{1/2}$ value, suggesting that 50µM is sufficient to elicit the full effect. Repeating the experiment with the addition of 15µM cAMP to the pipette solution did not produce any further shift in the activation curve, indicating that the synthetic peptide elicits a cAMP-like effect on the channel (Fig 4.25-C and -D).

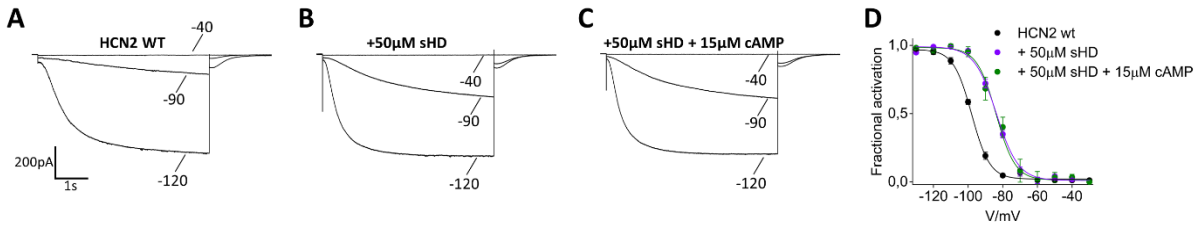

Figure 4.25: sHD peptide effect on mHCN2 channel.

***A-C**, Representative whole-cell currents recorded, at the selected indicated voltages, from HEK293T cells transiently expressing wild-type mHCN2 in the presence of 50µM of sHD alone (B) or in combination with 15µM of cAMP (C). **D,** Mean activation curve of wild-type HCN2 (black circles) in the presence of 50µM of sHD alone (violet circles) or in combinatrion with 15µM of cAMP (green circles). Lines show data fit to a Boltzmann function provding half activation potential (mean $V_{1/2}$ ± SEM) and inverse slope factor (mean k ± SEM) values as follow: $V_{1/2}$ = -97,9 ± 0,6 mV, k = 5,2 ± 1 (HCN2 wild-type); $V_{1/2}$ = -83,9 ± 0,6mV*, k = 5,5 ± 0,4 (+ 50µM sHD); $V_{1/2}$ = -83,7* ± 0,9mV, k = 6,3 ± 0,8 (+ 50µM sHD + 15µM cAMP). *p<0.05 One-way ANOVA with Fisher's test compared to HCN2 in control solution.*

Despite the fact that the mechanism of action of sHD was still unclear, we decided to verify if the peptide could be used to modulate native I_f current. Since HCN4 is the major molecular determinant that underlies the current in the sino-atrial node of the heart, we first tested the effect of sHD on rabbit HCN4 channel transiently expressed in HEK cells. The results are similar to those obtained in HCN2 channel: in the presence of 50µM sHD we measured a shift in the $V_{1/2}$ of 19,6 ± 0,8 mV (n=4) mV, which closely matches the effect elicited by cAMP in this isoform (Fig.4.26-A). Thus, in collaboration with the laboratory of Dr. Matteo E. Mangoni (Département de Physiologie Université de Montpellier, France) we tested the effect of sHD on the native I_f current in cardiomyocytes. The experiments were performed in whole-cell configuration in myocytes isolated from the sino-atrial node of adult mice. I_f currents were recorded with and without 50µM sHD in the pipette solution. Also in this case the synthetic peptide positively shifted the $V_{1/2}$ of 10 ± 2,2 mV (n=5) (Fig. 4.26-B). Notably, this is comparable to that induced by saturating concentration of isoproterenol [57] and closely matches the effect of β-adrenergic stimulation.

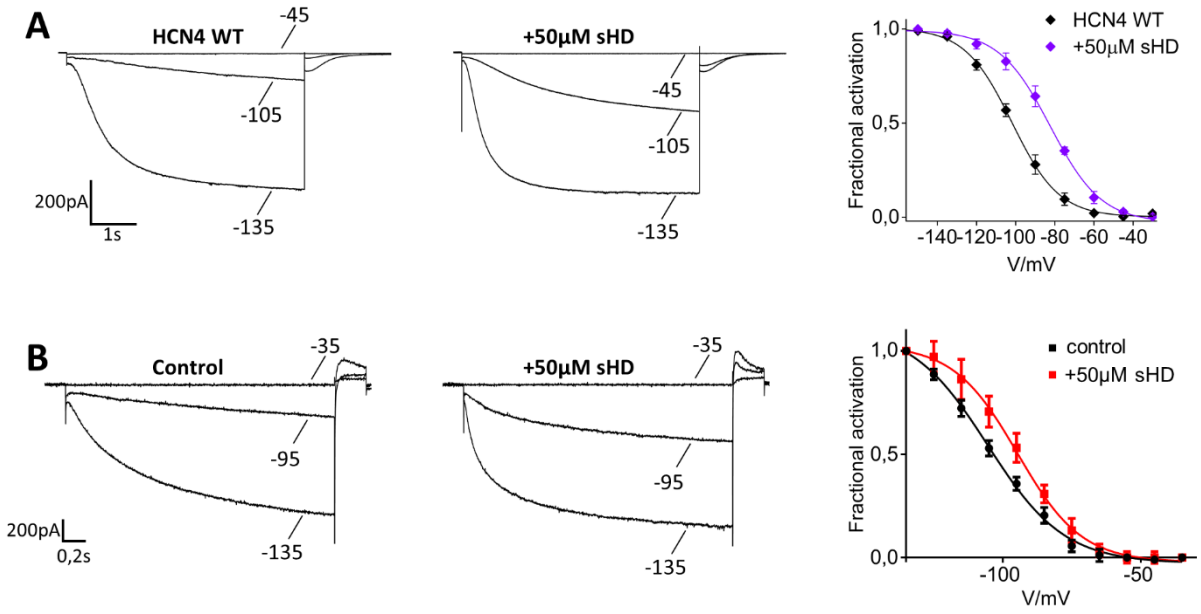

Figure 4.26: sHD effect on HCN4 (HEK cells) and native I_f current.
***A**, Representative whole-cell currents recorded, at the selected indicated voltages, from HEK293T cells transiently expressing wild-type RbHCN4 in the absence (left) and in the presence (centre) of 50µM of sHD. Right panel shows mean activation curve of wild-type HCN4 in the absence (black rhombus) and in the presence (violet rhombus) of 50µM of sHD. Lines show data fit to a Boltzmann function provding half activation potential (mean $V_{1/2}$ ± SEM) and inverse slope factor (mean k ± SEM) values as follow: $V_{1/2}$ = -101,9 ± 0,8 mV, k = 12 ± 0,6 (HCN4 wild-type); $V_{1/2}$ = -82,3 ± 1 mV*, k = 13 ± 0,9 (+ 50µM sHD). *p<0.05 by Student's t-test. **B**, Representative current traces of I_f current recorded, at the selected voltages, from SAN isolated myocites in the absence (left) and in the presence (centre) of 50µM sHD in pipette solution. Right panel shows mean activation curve plotted at the tail currents of I_f current recorded in the absence (black squares) and in the presence of 50µM of sHD (red squares). Lines show data fit to a Boltzmann function provding half activation potential (mean $V_{1/2}$ ± SEM) values as follow: $V_{1/2}$ = -105 ± 2 mV, (HCN4 wild-type); $V_{1/2}$ = -95 ± 1 mV*, (+ 50µM sHD). *p<0.05 by Student's t-test.*

Our data are still not sufficient to explain the molecular mechanism of action of the sHD on HCN channels. Nevertheless, the finding that in myocytes this small peptide mimics the modulatory effect of cAMP on the channel, opens, in our view, future applications of this tool for targeted therapeutic interventions.

5 CONCLUSIONS

In 1991 DiFrancesco and collaborators demonstrated that the I_f current of cardiac pacemaker cells is activated by the direct binding of cAMP to the cytosolic side of the channels by a mechanism that is independent from the phosphorylation. This represented the first evidence of a channel activated by membrane hyperpolarization and whose voltage dependent activation is further modulated by the direct binding of cAMP [33]. Starting from this first evidence several studies were designed to explain the molecular mechanism that allow this dual regulation. By combining electrophysiology and patch-clamp fluorometry techniques, some groups highlighted a role for the HCN channel VSD in the allosteric regulation of cAMP affinity for the CNBD, providing the first evidences of mechanism that directly couples the two elements without involving the gating of the pore [6], [7]. Despite providing significant advances in the knowledge of HCN channel structure-function relations, the Cryo-EM structure of HCN1 left the question of how conformational information is transmitted between the CNBD and the transmembrane portion of the channel. In this scenario we contributed finding, in the HCN domain, the key element that physically couples the C-terminal region of the channel with the transmembrane VSD, identifying the key residues that are directly involved in the transmission of the signal from the CNBD to the VSD. Hence, we propose that the C-linker rotation induced by the binding of cAMP to CNBD is directly transduced by the HCN domain in a little movement of the S4 voltage sensor helix via hydrophobic interactions. This little movement is of course too weak to open the pore, but allows the facilitation of the voltage dependence opening by lowering the energy (i.e. the voltage) required to move the voltage sensor helixes. Therefore, we suggest that the autoinhibitory effect of the CNBD, which constrains gating to more hyperpolarized potentials, is directly mediated by the HCN domain, that might limit or promotes the extent of the movement of the voltage sensor domain depending on the bound or unbound state of the CNBD. In agreement with our model there are both functional and computational data published in literature: basing on their functional results, Thon and collaborators proposed that ligand binding to the CNBD moderately promotes movement of the voltage sensor in a concentration dependent manner [6], [7]. More recently, using a

linear response theory (LTR) mechanical model of HCN channels, Gross and co-authors recently obtained the evidence that cAMP binding causes the tilting of all the voltage sensor helixes [58].

Our findings could also be related to the gating model proposed by Bell and Siegelbaum in 2004 [44]: they proposed that the tilting movements in transmembrane segments surrounding S4 cause the formation of a water-filled crevice (gating canal) at the level of the C-terminal tail of S4, whose motion was proposed to be coupled to the movement of the activation gate of the channel. The “second hydrophobic pocket” that we found to connect the HCN domain to the VSD is located exactly at the level of C-terminal tail of S4, where the gating canal should form; thus, we can suppose that, by influencing the conformation of the “second hydrophobic pocket”, the HCN domain might have a role in lowering or increasing the energy barrier of the formation of the internal gating canal, i.e. facilitating or antagonizing the channel opening.

Moreover, our results highlight an intriguingly difference between HCN1 and HCN2 isoforms: in HCN2 we found that a putative electrostatic interaction involving the HCN domain and (probably) the CNBD, is relevant for the modulation of the cAMP sensitivity. Interestingly, this interaction does not seem to exist in HCN1, where the mutation of the same residue of HCN2 did not caused any change. Therefore, our work provide also evidences that, despite the main regulatory mechanism are shared among the different isoforms, real differences exists within HCN1 and HCN2 channels, leading the basis for future investigations on how these channels can be so similar but at the same time so divergent. However, structural data of HCN2 followed by a functional validation are required to understand the meaning of this difference.

6 BIBLIOGRAPHY

[1] M. Biel, C. Wahl-schott, S. Michalakis, and X. Zong, “Hyperpolarization-Activated Cation Channels : From Genes to Function,” pp. 847–885, 2009.

[2] R. B. Robinson and S. a Siegelbaum, “Hyperpolarization-activated cation currents: from molecules to physiological function.,” *Annu. Rev. Physiol.*, vol. 65, no. 4, pp. 453–480, 2003.

[3] C. Lee and R. Mackinnon, “Structures of the Human HCN1 Hyperpolarization-Activated Channel,” *Cell*, vol. 168, no. 1–2, p. 111–120.e11.

[4] M. Baruscotti, A. Bucchi, R. Milanesi, M. Paina, A. Barbuti, T. Gnecchi-Ruscone, E. Bianco, L. Vitali-Serdoz, R. Cappato, and D. DiFrancesco, “A gain-of-function mutation in the cardiac pacemaker HCN4 channel increasing cAMP sensitivity is associated with familial Inappropriate Sinus Tachycardia.,” *Eur. Heart J.*, vol. 38, no. 4, pp. 280–288, Jan. 2017.

[5] C. Marini, A. Porro, A. Rastetter, C. Dalle, I. Rivolta, D. Bauer, R. Oegema, C. Nava, E. Parrini, D. Mei, C. Mercer, R. Dhamija, C. Chambers, C. Coubes, J. Thevenon, L. P. Ku, Š. Katalin, A. Laridon, E. Brilstra, B. Koeleman, L. J. R., F. Zara, P. Striano, A. Barbuti, D. DiFrancesco, E. LeGuern, R. Guerrini, K. Santoro, Bina; Hamacher, G. Thiel, A. Moroni, J. C. DiFrancesco, and C. Depienne, “HCN1 mutation spectrum: from neonatal epileptic encephalopathy to benign generalized epilepsy and beyond,” *Submitt. to Brain - Accept.*

[6] J. Kusch, C. Biskup, S. Thon, E. Schulz, V. Nache, T. Zimmer, F. Schwede, and K. Benndorf, “Interdependence of Receptor Activation and Ligand Binding in HCN2 Pacemaker Channels,” *Neuron*, vol. 67, no. 1, pp. 75–85, 2010.

[7] S. Thon, E. Schulz, J. Kusch, K. Benndorf, and F. Schmalkalden, “Article Conformational Flip of Nonactivated HCN2 Channel Subunits Evoked by Cyclic Nucleotides,” *Biophysj*, vol. 109, no. 11, pp. 2268–2276, 2015.

[8] C. Nava, C. Dalle, A. Rastetter, P. Striano, C. G. F. de Kovel, R. Nabbout, C. Cancès, D. Ville, E. H. Brilstra, G. Gobbi, E. Raffo, D. Bouteiller, Y. Marie, O. Trouillard, A. Robbiano, B. Keren, D. Agher, E. Roze, S. Lesage, A. Nicolas, A. Brice, M. Baulac, C. Vogt, N. El Hajj, E. Schneider, A. Suls, S. Weckhuysen, P. Gormley, A.-E. Lehesjoki, P. De Jonghe, I. Helbig, S. Baulac, F. Zara, B. P. C.

Koeleman, T. Haaf, E. LeGuern, and C. Depienne, “De novo mutations in HCN1 cause early infantile epileptic encephalopathy.,” *Nat. Genet.*, vol. 46, no. 6, pp. 640–5, 2014.

[9] H. Servatius, A. Porro, S. A. Pless, A. Schaller, B. Asatryan, H. Tanner, S. F. de Marchi, L. Roten, J. Seiler, A. Haeberlin, S. H. Baldinger, F. Noti, A. Lam, J. Fuhrer, A. Moroni, and A. Medeiros-Domingo, “Phenotypic Spectrum of HCN4 Mutations: A Clinical Case,” *Circ. Genomic Precis. Med.*, vol. 11, no. 2, Feb. 2018.

[10] C. Wahl-Schott and M. Biel, “HCN channels: Structure, cellular regulation and physiological function,” *Cell. Mol. Life Sci.*, vol. 66, no. 3, pp. 470–494, 2009.

[11] S. Moosmang, J. Stieber, X. Zong, M. Biel, F. Hofmann, and A. Ludwig, “Cellular expression and functional characterization of four hyperpolarization-activated pacemaker channels in cardiac and neuronal tissues.,” *Eur. J. Biochem.*, vol. 268, no. 6, pp. 1646–1652, Mar. 2001.

[12] L. A. Moosmang S, Biel M, Hofmann F, “Differential Distribution of Four Hyperpolarization-Activated Cation Channels in Mouse Brain,” *Biol. Chem.*, vol. 380, p. 975, 1999.

[13] B. Santoro, S. Chen, A. Luthi, P. Pavlidis, G. P. Shumyatsky, G. R. Tibbs, and S. A. Siegelbaum, “Molecular and functional heterogeneity of hyperpolarization-activated pacemaker channels in the mouse CNS.,” *J. Neurosci.*, vol. 20, no. 14, pp. 5264–5275, Jul. 2000.

[14] W. Shi, R. Wymore, H. Yu, J. Wu, R. T. Wymore, Z. Pan, R. B. Robinson, J. E. Dixon, D. McKinnon, and I. S. Cohen, “Distribution and prevalence of hyperpolarization-activated cation channel (HCN) mRNA expression in cardiac tissues.,” *Circ. Res.*, vol. 85, no. 1, pp. e1-6, Jul. 1999.

[15] E. A. Accili, C. Proenza, M. Baruscotti, and D. DiFrancesco, “From funny current to HCN channels: 20 years of excitation.,” *News Physiol. Sci. an Int. J. Physiol. Prod. jointly by Int. Union Physiol. Sci. Am. Physiol. Soc.*, vol. 17, pp. 32–37, Feb. 2002.

[16] D. DiFrancesco, “Pacemaker mechanisms in cardiac tissue.,” *Annu. Rev. Physiol.*, vol. 55, pp. 455–472, 1993.

[17] D. DiFrancesco and D. Noble, “The funny current has a major pacemaking role in the sinus node.,” *Hear. Rhythm*, vol. 9, no. 2, pp. 299–301, Feb. 2012.

[18] M. F. Nolan, J. T. Dudman, P. D. Dodson, and B. Santoro, “HCN1 channels control resting and active integrative properties of stellate cells from layer II of the entorhinal cortex.,” *J. Neurosci.*, vol. 27, no. 46, pp. 12440–12451, Nov. 2007.

[19] K. B. Craven and W. N. Zagotta, “CNG AND HCN CHANNELS: Two Peas, One Pod,” *Annu. Rev. Physiol.*, vol. 68, no. 1, pp. 375–401, 2006.

[20] J. C. Magee, “Dendritic Ih normalizes temporal summation in hippocampal CA1 neurons,” *Nat Neurosci*, vol. 2, no. 6, pp. 508–514, Jun. 1999.

[21] L. Sartiani, M. N. Romanelli, A. Mugelli, and E. Cerbai, “Updates on HCN Channels in the Heart: Function, Dysfunction and Pharmacology.,” *Curr. Drug Targets*, vol. 16, no. 8, pp. 868–876, 2015.

[22] J. C. DiFrancesco and D. DiFrancesco, “Dysfunctional HCN ion channels in neurological diseases,” *Front. Cell. Neurosci.*, vol. 6, p. 174, Mar. 2015.

[23] E. Gerard, P. Hochstrate, P.-W. Dierkes, and P. Coulon, “Functional properties and cell type specific distribution of I(h) channels in leech neurons.,” *J. Exp. Biol.*, vol. 215, no. Pt 2, pp. 227–238, Jan. 2012.

[24] V. Macri and E. A. Accili, “Structural elements of instantaneous and slow gating in hyperpolarization-activated cyclic nucleotide-gated channels.,” *J. Biol. Chem.*, vol. 279, no. 16, pp. 16832–16846, Apr. 2004.

[25] C. Proenza, D. Angoli, E. Agranovich, V. Macri, and E. A. Accili, “Pacemaker channels produce an instantaneous current.,” *J. Biol. Chem.*, vol. 277, no. 7, pp. 5101–5109, Feb. 2002.

[26] C. Proenza and G. Yellen, “Distinct populations of HCN pacemaker channels produce voltage-dependent and voltage-independent currents.,” *J. Gen. Physiol.*, vol. 127, no. 2, pp. 183–190, Feb. 2006.

[27] B. Santoro and G. R. Tibbs, “The HCN gene family: molecular basis of the hyperpolarization-activated pacemaker channels.,” *Ann. N. Y. Acad. Sci.*, vol. 868, pp. 741–764, Apr. 1999.

[28] B. J. Wainger, M. DeGennaro, B. Santoro, S. A. Siegelbaum, and G. R. Tibbs, “Molecular mechanism of cAMP modulation of HCN pacemaker channels,” *Nature*, vol. 411, no. 6839, pp. 805–810, Jun. 2001.

[29] A. Ludwig, X. Zong, M. Jeglitsch, F. Hofmann, and M. Biel, “A family of hyperpolarization-activated mammalian cation channels.,” *Nature*, vol. 393, no.

6685, pp. 587–591, Jun. 1998.

[30] D. DiFrancesco, “Block and activation of the pace-maker channel in calf purkinje fibres: effects of potassium, caesium and rubidium.,” *J. Physiol.*, vol. 329, pp. 485–507, Aug. 1982.

[31] X. Yu, K.-L. Duan, C.-F. Shang, H.-G. Yu, and Z. Zhou, “Calcium influx through hyperpolarization-activated cation channels (I(h) channels) contributes to activity-evoked neuronal secretion.,” *Proc. Natl. Acad. Sci. U. S. A.*, vol. 101, no. 4, pp. 1051–1056, Jan. 2004.

[32] G. Michels, M. C. Brandt, N. Zagidullin, I. F. Khan, R. Larbig, S. van Aaken, J. Wippermann, and U. C. Hoppe, “Direct evidence for calcium conductance of hyperpolarization-activated cyclic nucleotide-gated channels and human native If at physiological calcium concentrations.,” *Cardiovasc. Res.*, vol. 78, no. 3, pp. 466–475, Jun. 2008.

[33] D. DiFrancesco and P. Tortora, “Direct activation of cardiac pacemaker channels by intracellular cyclic AMP.,” *Nature*, vol. 351, no. 6322, pp. 145–147, May 1991.

[34] C. Ulens, S. A. Siegelbaum, W. Street, N. York, and N. York, “Regulation of Hyperpolarization-Activated HCN Channels by cAMP through a Gating Switch in Binding Domain Symmetry,” vol. 40, pp. 959–970, 2003.

[35] U. B. Kaupp and R. Seifert, “Molecular diversity of pacemaker ion channels.,” *Annu. Rev. Physiol.*, vol. 63, pp. 235–257, 2001.

[36] K. B. Craven and W. N. Zagotta, “Salt bridges and gating in the COOH-terminal region of HCN2 and CNGA1 channels.,” *J. Gen. Physiol.*, vol. 124, no. 6, pp. 663–677, 2004.

[37] K. S. Shin, C. Maertens, C. Proenza, B. S. Rothberg, and G. Yellen, “Inactivation in HCN Channels Results from Reclosure of the Activation Gate : Desensitization to Voltage,” vol. 41, pp. 737–744, 2004.

[38] S. Chen, J. Wang, L. Zhou, M. S. George, and S. a Siegelbaum, “Voltage sensor movement and cAMP binding allosterically regulate an inherently voltage-independent closed-open transition in HCN channels.,” *J. Gen. Physiol.*, vol. 129, no. 2, pp. 175–188, 2007.

[39] H. Pape, “Queer current and pacemaker: The hyperpolarization-activated cation current in neurons.,” *Annu. Rev. Physiol.*, vol. 58. pp. 299–327, 1996.

[40] E. C. Emery, G. T. Young, and P. A. McNaughton, “HCN2 ion channels: an emerging role as the pacemakers of pain.,” *Trends Pharmacol. Sci.*, vol. 33, no. 8, pp. 456–463, Aug. 2012.

[41] E. C. Emery, G. T. Young, E. M. Berrocoso, L. Chen, and P. A. McNaughton, “HCN2 ion channels play a central role in inflammatory and neuropathic pain.,” *Science*, vol. 333, no. 6048, pp. 1462–1466, Sep. 2011.

[42] C. Tsantoulas, E. R. Mooney, and P. A. McNaughton, “HCN2 ion channels: basic science opens up possibilities for therapeutic intervention in neuropathic pain,” *Biochem. J.*, vol. 473, no. 18, pp. 2717–2736, 2016.

[43] M. S. P. Sansom, I. H. Shrivastava, J. N. Bright, J. Tate, C. E. Capener, and P. C. Biggin, “Potassium channels: structures, models, simulations.,” *Biochim. Biophys. Acta*, vol. 1565, no. 2, pp. 294–307, Oct. 2002.

[44] D. C. Bell, H. Yao, R. C. Saenger, J. H. Riley, and S. A. Siegelbaum, “Changes in Local S4 Environment Provide a Voltage-sensing Mechanism for Mammalian Hyperpolarization–activated HCN Channels,” *J. Gen. Physiol.*, vol. 123, no. 1, pp. 5–20, 2004.

[45] R. Mannikko, F. Elinder, and H. P. Larsson, “Voltage-sensing mechanism is conserved among ion channels gated by opposite voltages.,” *Nature*, vol. 419, no. 6909, pp. 837–841, Oct. 2002.

[46] S. Vemana, S. Pandey, and H. P. Larsson, “S4 Movement in a Mammalian HCN Channel,” *J. Gen. Physiol.*, vol. 123, no. 1, pp. 21–32, Jan. 2004.

[47] W. N. Zagotta, N. B. Olivier, K. D. Black, E. C. Young, R. Olson, and E. Gouaux, “Structural basis for modulation and agonist specificity of HCN pacemaker channels.,” *Nature*, vol. 425, no. 6954, pp. 200–205, Sep. 2003.

[48] M. Lolicato, M. Nardini, S. Gazzarrini, S. Moller, D. Bertinetti, F. W. Herberg, M. Bolognesi, H. Martin, M. Fasolini, J. A. Bertrand, C. Arrigoni, G. Thiel, and A. Moroni, “Tetramerization dynamics of C-terminal domain underlies isoform-specific cAMP gating in hyperpolarization-activated cyclic nucleotide-gated channels.,” *J. Biol. Chem.*, vol. 286, no. 52, pp. 44811–44820, Dec. 2011.

[49] M. C. Puljung, H. A. DeBerg, W. N. Zagotta, and S. Stoll, “Double electron-electron resonance reveals cAMP-induced conformational change in HCN channels.,” *Proc. Natl. Acad. Sci. U. S. A.*, vol. 111, no. 27, pp. 9816–9821, Jul. 2014.

[50] A. Saponaro, S. R. Pauleta, F. Cantini, M. Matzapetakis, C. Hammann, C. Donadoni, L. Hu, G. Thiel, L. Banci, B. Santoro, and A. Moroni, “Structural basis for the mutual antagonism of cAMP and TRIP8b in regulating HCN channel function,” *Proc. Natl. Acad. Sci.*, vol. 111, no. 40, pp. 14577–14582, 2014.

[51] N. Tran, C. Proenza, V. Macri, F. Petigara, E. Sloan, S. Samler, and E. A. Accili, “A Conserved Domain in the NH 2 Terminus Important for Assembly and Functional Expression of Pacemaker Channels,” vol. 277, no. 46, pp. 43588–43592, 2002.

[52] Y. Pan, J. G. Laird, D. M. Yamaguchi, and S. A. Baker, “An N-terminal ER export signal facilitates the plasma membrane targeting of HCN1 channels in photoreceptors,” *Investig. Ophthalmol. Vis. Sci.*, vol. 56, no. 6, pp. 3514–3521, 2015.

[53] C. Viscomi, C. Altomare, A. Bucchi, E. Camatini, M. Baruscotti, A. Moroni, and D. DiFrancesco, “C Terminus-mediated Control of Voltage and cAMP Gating of Hyperpolarization-activated Cyclic Nucleotide-gated Channels,” *J. Biol. Chem.*, vol. 276, no. 32, pp. 29930–29934, 2001.

[54] A. Saponaro, F. Cantini, A. Porro, A. Bucchi, D. DiFrancesco, V. Maione, C. Donadoni, B. Introini, P. Mesirca, M. E. Mangoni, G. Thiel, L. Banci, B. Santoro, and A. Moroni, “A synthetic peptide that prevents cAMP regulation in mammalian hyperpolarization-activated cyclic nucleotide-gated (HCN) channels,” *Elife*, vol. 7, pp. 1–22, 2018.

[55] S. Chen, J. Wang, and S. a Siegelbaum, “Properties of hyperpolarization-activated pacemaker current defined by coassembly of HCN1 and HCN2 subunits and basal modulation by cyclic nucleotide.,” *J. Gen. Physiol.*, vol. 117, no. 5, pp. 491–504, 2001.

[56] J. Wang, S. Chen, and S. A. Siegelbaum, “Regulation of Hyperpolarization-activated HCN Channel Gating and cAMP Modulation due to Interactions of COOH Terminus and Core Transmembrane Regions,” *J. Gen. Physiol.*, vol. 118, no. 3, pp. 237–250, 2001.

[57] J. Alig, L. Marger, P. Mesirca, H. Ehmke, M. E. Mangoni, and D. Isbrandt, “Control of heart rate by cAMP sensitivity of HCN channels,” *Proc. Natl. Acad. Sci.*, vol. 106, no. 29, pp. 12189–12194, 2009.

[58] C. Gross, A. Saponaro, B. Santoro, A. Moroni, G. Thiel, and K. Hamacher, “Mechanical transduction of cytoplasmic-to-transmembrane-domain movements in a hyperpolarization-activated cyclic nucleotide-gated cation channel.,” *J. Biol. Chem.*, vol. 293, no. 33, pp. 12908–12918, Aug. 2018.